FCTUC

University of Coimbra
Faculty of Sciences and Technology
Department of Physics

Reconstruction of Echocardiographic Images for the Detection of Several Congenital Heart Defects

Sofia Antunes

Coimbra, 2010

Reconstruction of Echocardiographic Images for the Detection of Several Congenital Heart Defects

Sofia Antunes

A Thesis submitted for the degree of Integrated Master in Biomedical Engineering

Department of Physics

Faculty of Science and Technology, University of Coimbra

July 2010

Contents

List of Figures

List of Tables

Acknowledgments

There are many people who have been very important to me during this year, contributing to the work on my thesis or being by my side, believing always in me.

First of all I would like to thank my advisor José Silvestre, for his continuous support, being always there to give any advice and encourage me to accomplish any goal. A special thanks goes also to my co-advisor Jaime Santos, for his good tips and patience with me (and with my scientific papers).

I would like to thank the physicians of the pediatric hospital of Coimbra for all the support given: Dr. Eduardo Castela, Dr. Paula Martins, Dr. Isabel Cristina and a special thanks to Tech. Helder Costa.

The warmest thanks go to Mommy and Dad, for the unconditional support and encouragement to pursue my dreams. They were always by my side in all my decisions to build my future.

I want to thank my brother for sharing his experience and endeavors with me. He always listens to my complaints and frustrations, and tries to help me as best as he can.

The most special thanks to Fabi and Marco, two people that came at last in my life, but who believe in me like they know me for ages.

Last, but not least, I would like to thank the people who were essential during my five university years, my friends. Many thanks to André, Andreia, Carlos, Anita and Pedro to provide me with the best years of my life in Coimbra, you are my best friends!

Abstract

The purpose of this thesis was the research of a new segmentation method to detect and extract the heart cavities in echocardiographic images. To satisfy the clinical practice requirements, it is demanded that the segmentation algorithm is capable of providing reliable boundary extraction. This is crucial to the correct diagnosis of potential congenital malformations and diseases.

The proposed algorithm is based on Log-Gabor wavelets to detect symmetric features in the images, and a level set evolution in order to extract simultaneously all heart cavities in an accurate way. The formulation of the level set uses a new logarithmic based stopping function, which improved the boundary detection when compared to other level set methods.

Experiments were performed on echocardiographic images of children hearts. The validation of the algorithm included comparisons using state-of-art methods as the manual contours drawn by a trained physician, and the error quantification using similarity metrics.

Our method outperforms the state-of-art in echocardiographic heart segmentation, encouraging its future application in the clinical practice. This new segmentation method has potential to improve the performance of *3D* reconstruction algorithms, since the increased accuracy of the extracted heart contours simplifies its alignment in space and henceforth the recover of the *3D* structure.

Chapter 1

Introduction

The project described in this thesis emerged from a partnership between the department of physics, the department of electrical and computer engineering and the pediatric hospital of Coimbra. The objective is to research new methods to support the cardiologists in the analysis of echocardiographic images. The goal is to increase the accuracy of the diagnostic, improving the detection of congenital heart defects.

1.1 Context

Medical ultrasonography is an important tool for imaging the heart structures, since it is noninvasive, safety, portable and the images are available in real-time, and also the cost is low compared to other medical imaging techniques. Other reasons for its success are the information provided, which is very helpful in clinical diagnosis of heart diseases and the application in emerging areas such as image-guided interventions.

The echocardiographic examination is always done when it is suspected that the newborn (patient) has a heart disease. The abnormalities need to be diagnosed and followed in time by observing the heart chambers, walls motion, valves function, and estimating the volume of the cavities. Today, the analysis is performed visually by each physician who gives his own local interpretation.

In order to quantify the examination measures automatically, the heart boundaries need to be extracted. However, the problem of extracting the cavities from *2D* ultrasound images has revealed to be a hard task, since

echocardiographic images have low spatial resolution and high level of speckle noise. In addition, artifacts such as shadowing and attenuation due to the presence of the lungs complicate the analysis. These limitations lead to unclear or absent features of interest (the heart boundaries) that can be only estimated by the visual observation of the trained physicians.

Nowadays, echocardiographic instrumentation use semi-automatic approaches to determine the correct region of interest (ROI). However, it continues to be subjective and inter-observer dependent[1]. Fully automatic segmentation techniques would reduce this variability and provide clinical valuable information about the cardiac cavities and their respective volumes.

The *3D* echocardiography is a great advance in this imaging modality that offers the ability to improve and expand the cardiac diagnostic capabilities. The advantage over the *2D* visualization is surely the additional anatomic information provided and the ability to navigate within the volume. Another important advantage is the support in surgical planning, where surgeons may feel more confident with their interpretation of a *3D* view than with a set of 2D cross sections. Nevertheless, *3D* ultrasound still is object of investigation and development, due to economic and technological reasons as well as to insufficient convincement of the physicians. The *2D* echocardiography remains the standard system.

1.2 Scope of the Work

The echocardiography is the safest and most widely used imaging modality by pediatric cardiologists. However, it has some drawbacks e.g. ultrasound image segmentation is a difficult, inaccurate and time consuming task for the physicians. It is important to improve the diagnostic capabilities for an early detection of disease, with new automatic tools. The requirements are identified as being the following:

1. Low-cost addition

2. The practicality and simplicity should not be changed

In addition, to satisfy the clinical practice requirements, it is claimed that automatic segmentation algorithms are capable of providing reliable boundary extraction. Until now, the advances have been concentrated in the automatic

[1]Each physician has its own interpretation of the images.

segmentation of one heart chamber, the left ventricle (LV) as the most important heart cavity. The results however, are still not good enough to be applicable in the clinical practice.

The work was focused on the development of techniques to accurately segment the four heart cavities, due to its importance for the quantitative measures of the cardiac function (diagnostic tool). With a fully automatic and reliable segmentation method it would be possible to avoid all the manual measurements and to accurate reconstruct part of the heart in *3D*, helping to visualize details and planes that in *2D* images are not visible.

1.3 Main Contribution

The literature contains many works that attempt to segment automatically the left ventricle boundary of echocardiographic B-mode images. In the case of the four heart cavities, the studies are still less researched and the results are very poor, already in preliminary test phases.

This work gives a contribution in the segmentation of echocardiographic images. An automatic segmentation algorithm, based on the phase symmetry and contour evolution from a level set model, to extract simultaneously the four heart cavities is proposed. It is the first time that the phase symmetry and the level set model are used to segment the whole heart. The level set uses an alternative stopping function that increases the performance of the evolution at the heart boundaries.

1.4 Outline of the Thesis

This thesis is organized as follows. After this general introduction, chapter 2 proceeds with an anatomical overview of the heart, citing their most important structures such as the cavities and the valves. A short description of their physiology is given, mentioning the blood flows through the heart and the cardiac function. As the medical imaging equipments serve as tool to detect various defects, the most commonly newborn pathologies are named and described.

An explanation of the standard echocardiographic equipment is made in chapter 3, describing the image generation through the wave emission and reception used for the diagnostic purpose. The different imaging modes and standard views are presented with their correspondent drawbacks. In

addition, the new technologies using this imaging technique are reported.

Chapter 4 presents the state-of-art of left ventricle boundary extraction that was applied to *2D* echocardiographic images, including pre-processing approaches. The best techniques in the ultrasound segmentation environment were described as it is the case of level set and watershed. To conclude this chapter, some of the most important limitations of the presented techniques are reported.

The scientific contributions of this work are exposed in chapter 5, which describes the new segmentation method. The first step detects low level features, followed by the boundary extraction based on the level set model. Afterwards, the post-processing step is described to obtain four smoothed areas corresponding to the four heart cavities. As tool to quantify the algorithm error, several similarity metrics are exposed in this chapter.

The results are presented in chapter 6. A comparison among the different segmentation methods implemented is made. The performance of the different algorithms is studied and their values commented. Finally, the conclusions are formulated in chapter 7 with a summary and a discussion of future work.

1.5 Publications

The material in this thesis is based on work that has been published during this year in different international conferences (NDT, ICIAR and CISTI) and on a submission for the scientific journal *UltraSound in Medicine and Biology*.

For the European Conference of Non-Destructive Testing (Moscow) the usefulness of two methods were compared, namely the piecewise constant active contour model proposed by Chan and Vese, and the new variational level set formulation proposed by Chunming Li. Important parameters like shape and size of the initial contours, position in the images and propagation direction of the level set were tested. An evaluation of the performance of the two algorithms in terms of convergence time, different initialization masks, and smoothing techniques was done.

In the International Conference on Image Analysis and Recognition (Póvoa de Varzim), the automatic segmentation method that extracts the four heart cavity boundaries was exposed. The new pre processing algorithm based on phase symmetry and the contour convergence of the level set model were explained. Experimental results using real echocardiographic images of children have shown good performance of the method, providing a reliable tool

to segment the heart walls that could be helpful for clinical practice.

The just mentioned article was completed in the *Conferência Ibérica de Sistemas e Tecnologias de Informação* (Santiago de Compostela). In this work, the performance of the proposed method was quantitatively compared with three alternative level set functions and the watershed transform. The comparison was made using as reference manual drawn contours by physicians, having as evaluation tool two similarity metrics.

Chapter 2

The Heart

This chapter gives an overview of the heart anatomy and physiology, which is important to understand the information provided by echocardiographic examination. The most commonly pathologies related to congenital malformations are also mentioned.

2.1 Anatomy and Physiology

The function of the heart is to pump the blood through the entire body. It is localized in the thorax region, between both lungs protected by the sternum. Externally, it is covered by the pericardium and internally by the endocardium, being composed by miocardium, the cardiac muscle tissue.

This organ is functionally divided into two parts, the left and the right, which are separated by a muscular wall called the septum. Each side consists of two chambers: a thin walled chamber of blood, the atrium, and a thick walled camera to eject the blood, the ventricle. The right side receives blood from the veins and pumps blood through the pulmonary circulation, which carries venous blood to the lungs, while the left side of the heart pumps blood through the systemic circulation which carries oxygenated blood to all tissues of the body and returns the deoxygenated blood to the heart.

The heart's activity is involuntary and rhythmic, distinguishing states of cardiac muscle contraction and states of relaxation, stimulated by electrical impulses from the sinoatrial node. The time during which ventricular contraction occurs is called systole and the ventricular filling (relaxation phase)

is known as diastole. In the systole the blood leaves the heart with a maximum pressure on the walls of arteries that receive it, being called blood pressure.

A thick bundle of muscle crossing the right ventricle can be present, varying in size. It arose from the apical end of the right ventricle and connects the base of the anterior papillary muscles to the inter-ventricular septum, known as moderator band. It was thought to prevent overdistention of the ventricle, more recent research however, has indicated that it is part of the electrical conduction system of the heart [1].

A Cardiac cycle refers to the repetitive pumping process that begins with the onset of systole and ends with the beginning of the next systole. The heart contracts usually between 60-80 times per minute [2]. In the cardiac cycle, blood flows from the superior and inferior vena cavae to the right atrium, flowing across the tricuspid valve into the right ventricle. From here the blood moves into the pulmonary artery and after oxygenation in the lungs returns to the heart via four pulmonary veins that enter the left atrium. Across the mitral valve the blood flows from the left atrium into the left ventricle and is ejected through the aortic valve into the aorta (see Figure 2.1). The tricuspid and mitral (bicuspid) valves are known as the atrioventricular valves because they join the atrium with the ventricle of each side. The other type of valves, aortic and the pulmonary are called semilunar valves. The function of the heart valves is to maintain the unidirectional flow of blood by opening and closing depending on the difference in pressure on each side.

2.2 Pathologies

The congenital heart defects (CHD) are one of the most common malformations, being present in 1 of every 100 newborns [4] and are the principal cause of birth deaths. It refers to disease in the structures of the heart such as the valves (they may not fully open or close) causing blood to leak back into cardiac chambers or requiring heart chambers to contract more forcefully to move blood across the valve. The most frequently detected CHD is the ventricular septal defect, characterized by the flow of the oxygen rich blood from the left to the right side of the heart through the opening in the septum. The oxygen rich blood mixes with oxygen poor blood in the right side (see Figure 2.2). Other type of defects are related to the abnormal heart rhythm (such as long QT syndrome); Hypoplasia, which typically results in the failure of either the right ventricle or the left ventricle and obstruction of blood vessels [5]. Echocardiography plays a fundamental role in the cases where a

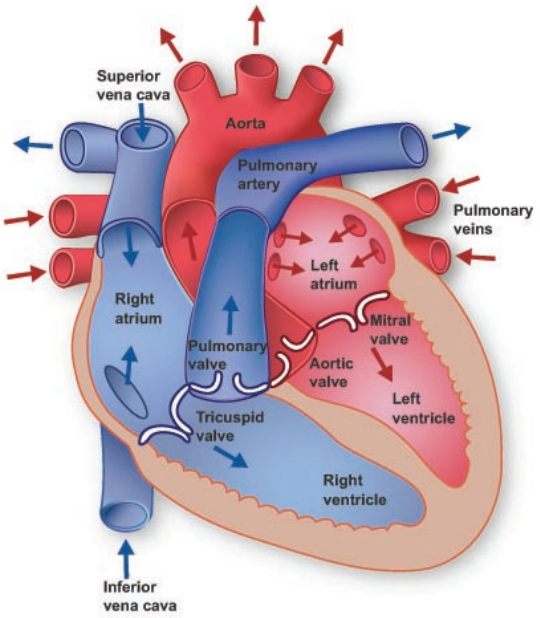

Figure 2.1: Heart Anatomy - the oxygen rich blood is represented in red and the oxygen poor blood in blue [3].

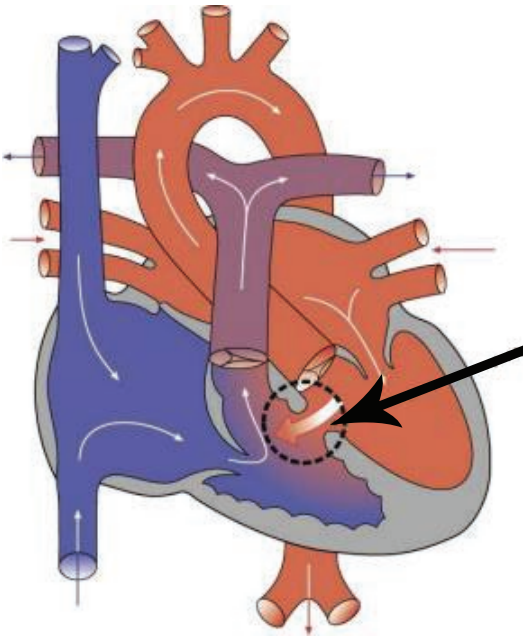

Figure 2.2: Heart Disease - ventricular septal defect [6].

disease is suspected, providing morphological and functional information of

the heart. The detail of the information is essential for a better understanding of the pathology, for choosing the appropriate therapeutic strategy, and if that is the case, for an appropriate surgical planning. Some of the mentioned wall defects may be treated through percutaneous closure, where the previous echocardiographic parameter analysis is essential to determine the feasibility of the procedure. Respecting to aorta coarctation, 3D echocardiography permits endoluminal reconstructions of the coarctation and dynamic measurements of the lesion during the cardiac cycle.

If a patient is suspected to have a heart failure, quantitative measurement of cardiac function is a critical step in the evaluation and management of the disease. The cardiac function is related to the atriums and ventricles shape attributes such as the thickness and motion of the walls and the respective enclosed area. The diagnostic is done evaluating some important parameters such as the end-diastolic and end-systolic volume, the ejection fraction of the left ventricle, and the pressure-volume ratio.

Chapter 3

Echocardiographic Equipment

Standard echocardiography is an important basic tool in the clinical practice for the quantitative analysis of cardiac function, wall motion and to measure blood flow in vessels. Compared to other imaging modalities, it has a prominent place as a routine clinical test, for many practical and safety reasons: it is non-invasive, portable, less expensive, and produces real time anatomical information without ionizing radiation.

The experts study the information provided by the echocardiography in a qualitative and quantitative manner, considering some particular alterations of the chamber shape, size and wall motion but also blood and myocardial velocities based on the Doppler shift.

The scanners consist of a phased-array transducer connected to the signal processing box. The acquired reflected signals are reconstructed and the image is displayed in real time on the monitor (see Figure 3.1).

3.1 Transducers

In medical imaging, the common acquisition method is the electronic scanning with a *1D* array transducer. The numerous and small crystals contained in the probe can be excited independently using a linear array or a phased-array. In the case of the linear array transducer, the ultrasonic beam is moved linearly by firing its elements sequentially. In cardiology however, the phased-array transducer is essential due to the small acoustic window of the heart. Its crystals are closer together and are activated with small timing (phase) differences, enabling to change the direction of propagation

Figure 3.1: An example of echocardiographic equipment [7].

of the wave and so focusing on arbitrary points at each direction [8]. Scanning through the body with numerous adjacent acoustic waves enables to form cross sectional images of the heart. In the case of the phased array, the sector format produces a sectorial image as shown in Figure 3.2. The probe is composed of piezoelectric crystals that produce, transmit and receive ultrasound waves. Each transducer converts electric energy into short length mechanical vibrations and transmit them into the heart through physical contact with the skin. Whenever the beam encounters boundaries and different surfaces or structures, it suffers reflection or scattering that returns to the transducer. Now, the transducer works in the reverse way, i.e., converts the mechanical vibrations into electric pulses. After all of the echoes from the first beam are received, a second line of data will be acquired adjacently, with a delay imposed on the probe. This process is repeated until it gets over 250 lines, typically. To form each line, 100-300μs are required and the complete image is formed in tens of milliseconds allowing the study of dynamic *2D* images.

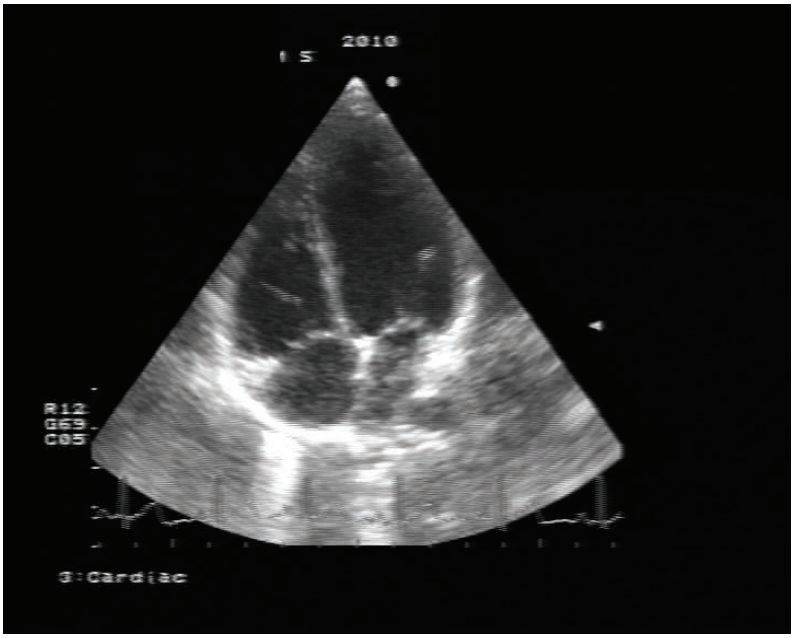

Figure 3.2: An example of an echocardiographic sectorial image.

3.2 Wave Propagation

Mechanical waves are generate by the piezoelectric crystals of the transducer, which undergo an expansion or contraction according to the polarity of the field. They are transmitted into the heart using ultrasound frequencies in the approximate range of 2 to 4 MHz. The probe comes in contact with the skin using a gel to allow maximum energy transmission. During the propagation through the soft tissues, at an approximate speed of 1540 m/s, reflection of the sound will occur on the interface of two different tissues, when the sound wave crosses from a medium to another medium of different impedance. The intensity of the reflected (and transmitted) wave at the interface depends on the acoustic impedances (Z) of the two tissues. The impedance is defined as $Z = \rho \times c$, where ρ is the density of the material and c the respective velocity of the sound waves. As the difference in Z for two media increases, higher intensity reflections will occur. The ability to discern an ultrasound image depends on the difference in acoustic impedance of the various body tissues (Table 3.1). The air has acoustic properties significantly different from tissues, reflecting a large portion of the signal back to the transducer, therefore the importance of using the gel between transducer and skin. When the ultrasound wavelength is comparable with the size of the encountered particles, each of them acts as a point source producing

spherical wavelets (Huygens's principle), then occurring a different reflection known as scattering. If the wave crosses the interface of two mediums at an oblique angle, refraction occurs, and during the propagation through the soft tissues, part of the energy will be absorbed[1] making gradual attenuation of the intensity of the beam. The attenuation is dependent on the density of the medium and is a function of the wave frequency. In the reverse process, when

Table 3.1: Acoustic impedance and velocity of sound values of the different body components [8].

Material	Acoustic Impedance, Z $(\times 10^6 kg/m^2 seg)$	Velocity of Sound, c (m/seg)
Air	0.0004	330
Soft Tissue	1.70	1540
Bone	7.80	3500
Fat	1.38	1450
Blood	1.61	1550
Muscle	1.70	1580
Water	1.48	1480

the backscattered waves hit the crystal, causing mechanical deformation, a potential difference will appear in the electrodes of the transducer. The magnitude of the potential difference developed in this form is proportional to the applied pressure.

Contrast, signal intensity and noise characteristics are all determined by the propagation properties through the tissues, by the energy loss and interactions that give rise to the backscattered signals.

3.3 Display Modes

The received pulse-echoes can be displayed in three basic scan modes: A, B and M.

The A-mode or amplitude mode is an *1D* scan display, where the information is visualized in terms of amplitude *versus* time. Thus, in general the x axis represents the propagation time of the ultrasounds and the y axis the

[1] converted into heat

amplitude of the collected echo. It is very useful for an accurate measurement of the heart structures dimensions.

In the B-mode or brightness mode, a *2D* image is produced through a cross section of a heart plan. It consists of consecutive A mode scan lines generated side by side, where each pulse corresponds to one line. The brightness of the image, in 256 gray levels, is proportional to the amplitude[2] of the echoes returned to the transducer. The larger the reflection is, the brighter the line will be. The *2D* image is formed from multiple equal spaced B-scan lines in the desired scan plane done electronically, using the phased array transducer. This display mode is used by convention in the diagnosis, to study both stationary and moving heart structures. It is possible to image with rates up to 40 frames per second, due to the high velocity of sound in soft tissues and the rapidly acquisition of a complete image. This allows dynamic imaging and a real time motion analysis.

The M-mode or motion mode provides information of tissue movement. It consists in displaying continuous series of A-mode scans on a selected cross section of the B-mode image as shown in Figure 3.3. A continuous time ramp is applied to the horizontal axis to display how the positions of the objects vary with time. It is a fundamental tool to detect the motion of the heart valves and heart wall against time, to quantify the heart chamber dimensions, systolic and diastolic, heart wall thickness, valvular movements and left ventricle functional indices.

3.4 Standard Views

Acoustic shadowing occurs when the emitted ultrasound pulse is greatly attenuated by strong reflectors like bone or lung that are impenetrable to ultrasounds. Indeed, the heart is covered by structures such as the intercostals and lung tissue, making the insonification a difficult task due to the limited acoustic window. Despite such difficulties, diagnostically useful images are still obtainable by careful selection of good visualization planes of the heart. In practice, experts have standard views for qualitative assessment of the structural, anatomical, and functional performance of the heart, for discovering and studying the abnormalities.

When the transducer is aligned in a sagittal orientation, this is termed a long axis view. The transducer is then turned 90 degrees, obtaining a cross section, termed short axis view. The mentioned views include parasternal

[2]The amplitude of the displayed signal in the A-scan is converted to a proportional intensity.

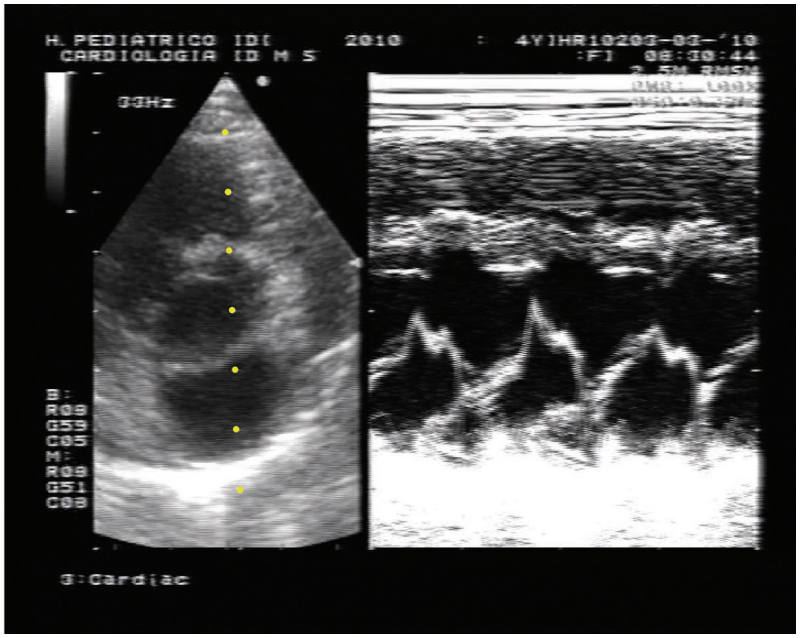

Figure 3.3: B-mode image (left) and M-mode representation (right) of the cross section selected, dot line, over the B-mode image.

short axis with three commonly used slices: at the level of the mitral valve, at the level of the papillary muscle, and at the apex between the papillary muscles and apical tip; parasternal long axis, apical 2-chamber long axis, and apical 4-chamber long axis. Two examples of such views are given in Figure 3.4.

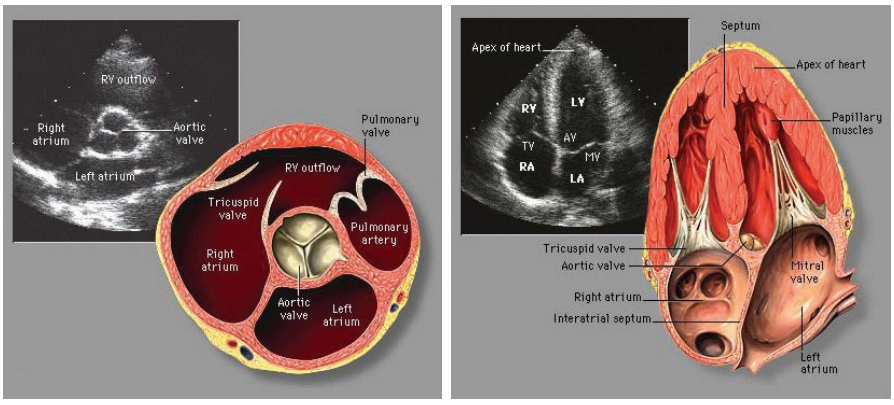

(a) Parasternal Short Axis (b) Apical 4-Chamber

Figure 3.4: Examples of two standard echocardiographic views [9].

3.5 Three Dimension Imaging

The ability to view a given volumetric image in a number of different planes gives more accurate measures about tissue malformations and small pathologies, providing also a good visualization of the septal defects. That enables the physician to evaluate the action to be developed in order to proceed with the required intervention to fix the injured structures. Also, in the case of valvular malformation it offers intracavitary perspectives of the valves, allowing a detailed analysis of their morphology, as well as coaptation mechanism and valvular regurgitation whether present.

3D Ultrasound is today the main research field in the echocardiographic imaging modality. There exist two commonly ways to produce *3D* echocardiography: mechanically or manually scanning a *1D* phased array transducer. Nevertheless, the number of *2D* slices that can be acquired per second is limited by the frame rate and the velocity of the sound, and this way *3D* acquisition cannot be accomplished in real time. Using a *2D* phased array transducer allows electronically steering of the symmetrically focused ultrasound beam throughout a volume. However, this transducer has a great dimension being still impracticable in the cardiology, due to the small acoustic window.

3D imaging is still far from a standard usage in clinical practice due to its unsatisfactory results. Another important aspect being investigated is related to the probe. Most of the systems used today have the transducer composed by a piezoelectric crystal but silicon is appearing as a very promising alternative capable of providing enhanced *4D* ultrasound images.

3.6 Doppler Effect

An important diagnostic tool is the Doppler mode. It is used in every echocardiographic examination to measure blood flow in vessels and valves, namely in the communication between the left and the right side of the heart and for detecting and evaluating regurgitation through the valves. It is based on the backscattering from the blood, being possible due to the red cells of the blood vessels which approximate or move away from the probe at different speeds. As the sound waves reach the blood vessels, they are reflected on these globules and return to the probe suffering a variation in frequency,

dependent on the magnitude and direction of the blood flow velocity:

$$\nu = \frac{f_D \cdot c}{2f_0 \cdot \cos(\alpha)} \tag{3.1}$$

where ν is the blood velocity, c the sound velocity in tissue, f_0 is the transmitted frequency, f_D is the Doppler shift of reflected ultrasound and α the insonation angle between the ultrasound beam and the direction of motion (velocity vector). The variation on the frequency is dependent on the incident wave angle. Greater frequencies are observed when the beam is parallel to the axis of the blood vessels and lower values when the incident beams are perpendicular to the vessel axis.

A way to display graphically is called the spectral Doppler, shown in Figure 3.5. Another technique to visualize the echo signals, is to present they as a color coded map overlaid on the B-mode image (color Doppler). The blood flowing to the probe has the color set to red and in the opposite case, when the flow moves away from the probe the color is blue. Other form to display the Doppler information is in the audible range, the power Doppler.

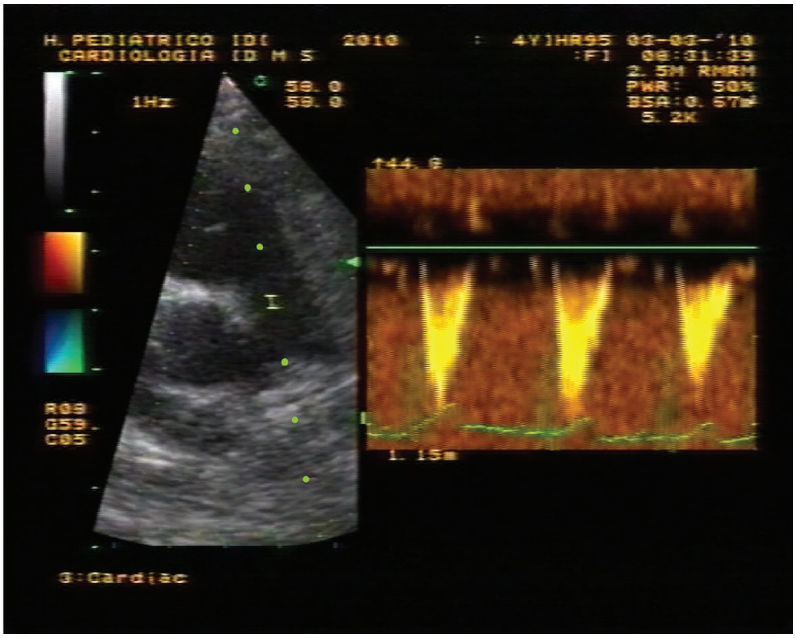

Figure 3.5: On the left, a *2D* image showing the placement of the Doppler sample (dot line) and on the right, Doppler frequency shift waveforms.

3.6.1 Wave Emition Modes

In the continuous wave Doppler, elements of the probe are divided into two groups: one for the continuous transmission and the other for the simultaneous reception. In this mode, only large flow velocities can be analyzed without ambiguity and therefore it is used for an accurate measurement of elevated blood flow velocities.

The pulsed wave Doppler alternates the emission and the reception of the short pulses. A small segment along the ultrasound beam is selected, on the B-mode image, and in this region the blood flow direction and velocity is measured. It is used to locate a specific region of abnormal flow, being unable to accurately measure high blood flow velocities.

3.7 Artifacts

Various artifacts and error sources in the generation of echocardiographic images affect their quality and accuracy, which can be inherent to the nature of the imaging modality or characteristic of how the system is implemented. In the ultrasound systems, as already mentioned, the speed of sound is assumed to be constant. However, the speed varies from 1450m/s to 1750 m/s in fat tissue and tendons respectively, varying also with temperature and tissue condition (Table 3.1). The assumed average value is 1540m/s. This inaccurate measurement of the speed of sound results in a wrong placement of the interfaces in the image, distorting the shape of the objects.

Not all the transmitted acoustic energy propagates in the exactly perpendicular direction to the transducer surface, generating minor ultrasound waves that travel in a different direction, known as side lobes. If these waves are great enough, they could create echoes, producing also artifacts in the B-mode image [10].

Speckle noise, the typical granular appearance of ultrasound images, is the result of constructive-destructive interference of the backscattered pulses from the small tissue components (multiple reflectors). Speckle can severely degrade the clinical information content of the images and makes filtering techniques for the noise reduction difficult to implement.

When acoustic shadow occurs, the ultrasounds give rise to dark areas or holes in the image. The opposite of this phenomenon is enhancement, corresponding to regions with low attenuation coefficient that originate echoes of high amplitude, identified in the image as bright regions. Reverberation occurs also when the ultrasound waves interacts with either bone or air, where

very strong reflectors close to the transducer surface produce multiple reflections, justifying the importance of using gel as a coupling medium between the probe and the skin.

Chapter 4

Ultrasound Image Segmentation

Image segmentation is a fundamental step in image analysis. It consists in the partition of the image in various sub-regions based on specific constrains. In the case of echocardiographic apical 4-chamber long axis images, the ROI consists in the four cardiac chambers. The purpose of segmentation in this case is to extract the four cavity boundaries. This first section gives an overview of segmentation methodologies specifically developed for the B-mode images. The following sections discuss active contour methods and watershed technique, which have been widely tested on these type of images.

4.1 An Overview

Conventional segmentation techniques such as thresholding or region growing are usually unsatisfactory, due to the noise of ultrasound images. Other traditional feature detectors like the Sobel or the Canny operators are not a good solution because they are unable to produce closed boundaries[1]. More advanced techniques have been proposed to improve the *2D* image segmentation procedure by the development of sophisticated algorithms [10] [11].

[1]It is fundamental that the segmentation algorithm finds four closed contours, corresponding to the four heart cavities.

Additional pre-processing and post-processing techniques are required as well as considerable *a priori* information about the objects of interest.

Pre-processing techniques recently applied for the noise reduction in the echocardiographic images include adaptive filtering [12], bayesian networks [13], adaptive wavelet thresholding [14] and other techniques such as Wiener filtering [15]. It has also been demonstrated that local phase-based methods are a good choice for the pre-processing step of ultrasound images [16], since they are unaffected by speckle and low contrast on the feature detection process.

The authors who have developed the most significant segmentation methodologies focused on B-mode images are, among others:

- *Jarur* and *Mora* [17] that use artificial neural network based on a self-organizing map (SOM) for the training, suitably classifying an image sequence of similar characteristics (see Figure 4.1).

(a) Original Image (b) Interior class (c) Edges of interior class (d) Edges after improvements

Figure 4.1: Cavity detection of *Jarur*'s work [17], with artificial neural network for an apical 2-chamber long axis image.

- *Suphalakshmi et al* [18] use fuzzy sistems supported by texture properties, where the formation of open contours appears as a significant drawback as shown in Figure 4.2.

- *Bansod et al* [19] optimize a radial search based algorithm with multi-frame guided local search to incorporate the temporal information (Figure 4.3). However, this is a semi-automated approach since it requires user interaction.

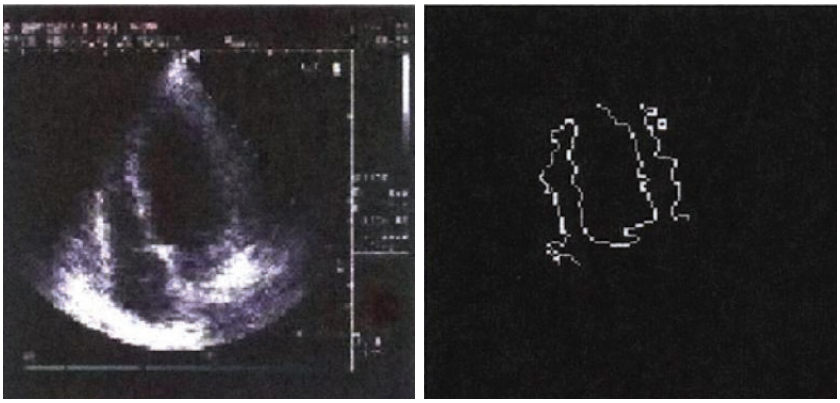

(a) Original Image (b) Segmentation Output

Figure 4.2: *Suphalakshmi*'s segmentation algorithm [18] on a long axis end systole image.

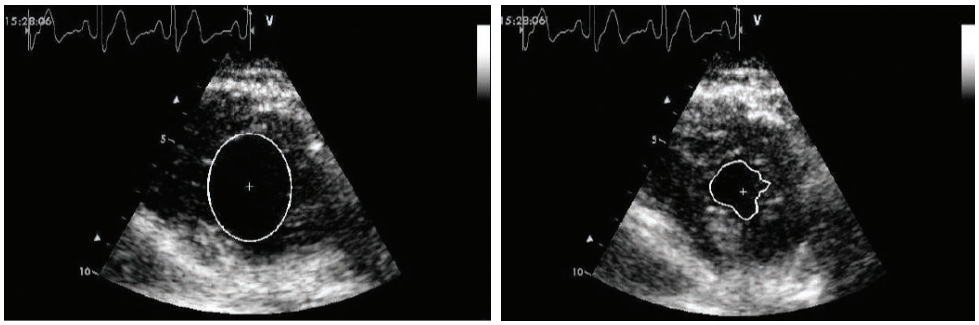

(a) Initialization, first frame (b) Guided local search based contour determination on the last frame

Figure 4.3: Apical short axis image segmentation using the radial search based method of *Bansod* [19].

- *Stoitsis et al* [20] use the Hough Transform as initial estimation for the active contour model (see Figure 4.4), based on the gradient vector flow field to automatically extract the carotid artery from sequences of B-mode images. The performance of their active contours was analyzed by comparing the extracted boundaries with the ones traced manually by an expert.
- *Valdes-Cristerna et al* [21] use a mean shift filter as pre-processing approach. Then, the regions obtained with this filter were used to define the initial contour of the active contour step, as shown in Figure 4.5.

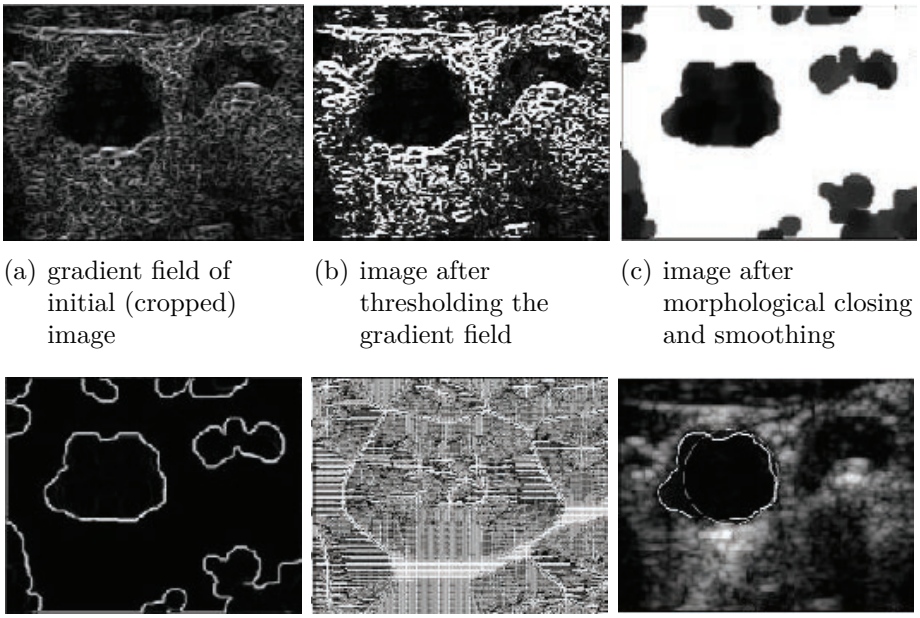

(a) gradient field of initial (cropped) image

(b) image after thresholding the gradient field

(c) image after morphological closing and smoothing

(d) image after gradient operator on gradient field

(e) gradient vector flow field

(f) the result shown on the original image (solid line)

Figure 4.4: Examples of the results of individual steps of the HT-initialized active contours methodology proposed by *Stoitsis* [20].

- *Cheng et al* [22] suggested a boundary detection method for long-axis images, using a markov random field model, the local statistics and a level set method to ensure that the resulting boundary is continuous and smooth (Figure 4.6). It was observed high correlation between the extracted boundaries and the expert-drawn ones.

4.2 Level Set

Active Contour models are today widely used to detect boundaries in medical images, due to its ability to smooth the speckle-induced error. *Kass et al* [23] were the first to propose an active contour model based on an energy minimization scheme[2]. An important drawback related to this classical

[2]Energy minimizing spline (snake) deforms from its initial cloused curve based on external constraint and image forces. The goal is to find the best fit between the snake and the shape of the object to be segmented.

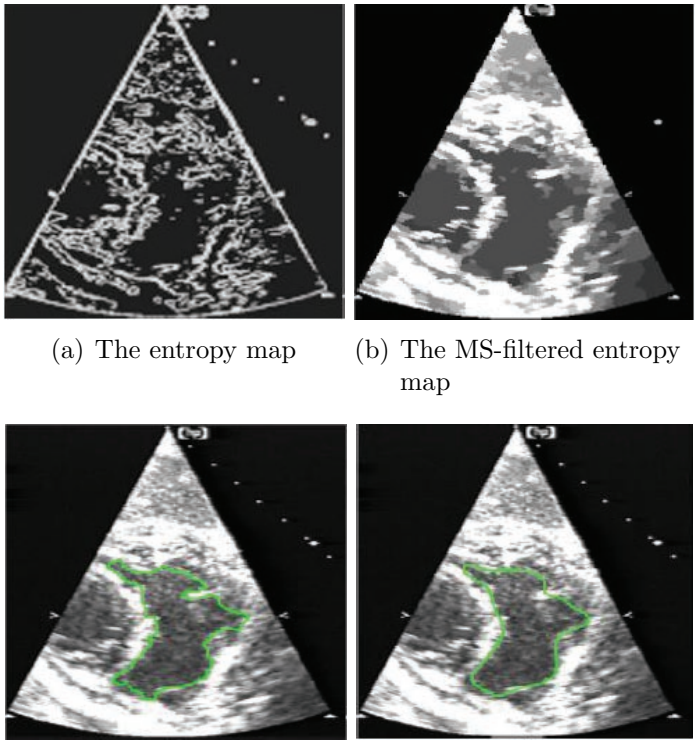

(a) The entropy map (b) The MS-filtered entropy map

(c) The initial contour fed to the snake (d) The final estimated contour

Figure 4.5: Segmentation results applying the algorithm of *Valdes-Cristerna* [21].

(parametric) approach is its inability to split and merge that is fundamental for the detection of more than one ROI in an image.

A more flexible and convenient solution was proposed by *Caselles et al* [24], known as geometric active contour model. It overcomes the restriction imposed by the traditional active contours. The concept of geometric deformable models was introduced by *Osher and Sethian* [25], proposing an implicit formulation of the previous described technique, known as level set. That formulation can handle complex shapes and topological changes.

The main idea of the level set is to minimize a function solving the corresponding partial differential equation (PDE). The method evolves a contour (*2D*) or surface (*3D*) implicitly by manipulating a higher dimensional function $\phi(x, y, t)$, where ϕ can evolve from its initial stage to the image boundaries based on a speed function that controls the contour evolution. Depending on the implementation scheme, it uses various properties of the image for the contour evolution process that can be based on image borders (edges) or on uniform areas (regions) or on both. The evolving contour is

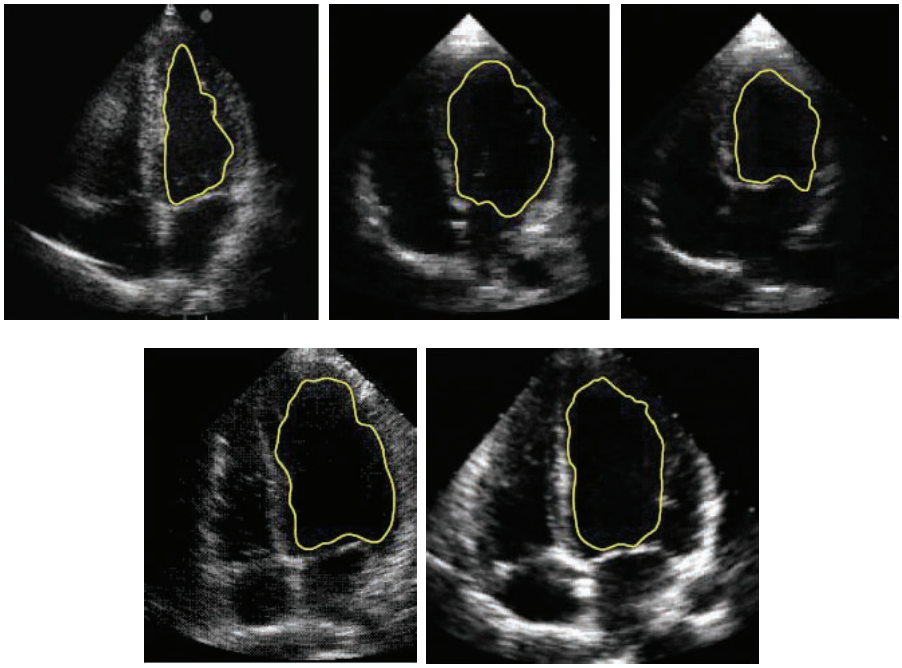

Figure 4.6: Results of LV boundary detection from different sequences with the method proposed by *Cheng et al* [22].

then extracted from the zero-level curve of $\phi : C = \{x|\phi(x) = 0\}$. The general curve evolution PDE in the level set framework is:

$$\frac{\partial \phi}{\partial t} = \mid \bigtriangledown \phi \mid F \tag{4.1}$$

where F is a speed function designed for the boundary detection. The level set function ϕ and the evolving curve C at the zero-level change together with time. The speed function F has different behaviours depending on the applied evolution methodology.

4.2.1 Edge Based

Whenever the velocity term F of the level set equation is based on the image edges, the model is called edge based. Most edge based active contour models consist of two parts: the regularity part determining the shape of contours, and the edge detection part to attract the contour towards the

edges:

$$F = [div(\frac{\bigtriangledown\phi}{|\bigtriangledown\phi|}) + \nu]P \tag{4.2}$$

where the term ν is an outward growing force, providing a fast convergence and $div(\frac{\bigtriangledown\phi}{|\bigtriangledown\phi|})$ is the curvature term. The stopping function P is responsible for attracting the contour to the image boundaries, being positive on homogeneous regions and having values near zero on the sharp edges. It was initially proposed by *Caselles et al* [24], which demonstrate the segmentation capabilities using this term on artificial and real medical images. The stopping term is defined as:

$$P = \frac{1}{1 + ||\bigtriangledown (G_\sigma * I)||} \tag{4.3}$$

and uses a function of the image gradient, i.e., a convolution of the intensity image with a Gaussian filter. That classical function presents some disadvantages, namely the edge stopping function never equals zero and the moving curve may cross the boundaries of the object.

Mora et al [26] proposes an alternative stopping term based on a coefficient of variation in order to develop a more efficient edge detector. Such a parameter controls the motion of the moving contours, being equal to zero at the edges. This alternative stopping term is characterized by a great robustness to speckle. The obtained results proved more reliability in detecting the heart cavities than the classical image gradient term.

Fang et al [27] incorporate temporal information into the level set functional to solve the problem of the frames with poor heart boundaries definition. They used a block matching technique to efficiently estimate the location of the heart beating. A comparison was made between the results of their methodology with the conventional level set edge-based method and the region based model using as reference the ground truth drawn by the clinicians, concluding that the method can successfully prevent the leakage problem of the heart boundaries present in some frames.

4.2.2 Region Based

In the region-based methodology, the region information of the target objects is used without image gradient related terms. *Mumford* and *Shah* [28] proposed this alternative active contour model. The segmentation relies on the statistical information of the image intensity, to minimize an energy func-

tion instead of searching edges. Using the Mumford and Shah segmentation model, *Chan* and *Vese* [29] proposed a method that is a particular case of the minimal partition problem, where the velocity term F is restricted to piecewise constant functions. Thus, it is possible to separate the image background from the image foreground. The authors replace the gradient term $| \bigtriangledown \phi|$ by the regularized Dirac functional $\delta(\phi)$ to remain close to the minimization problem:

$$\frac{\partial \phi}{\partial t} = \delta(\phi)[\lambda_2(I - \mu_{out})^2 - \lambda_1(I - \mu_{in})^2 - \alpha + \beta(div(\frac{\bigtriangledown \phi}{| \bigtriangledown \phi|}))] \tag{4.4}$$

where the first two terms of F: λ_1 and λ_2 measure variations inside/outside the active contour; the area inside the contour is given by the third term α, and the length of the curve is measured by the fourth term. The last two ones are regularization terms. Since medical images may have complex backgrounds, the use of the thresholds μ_{in} and μ_{out} can fail. Indeed, their global nature is based on the assumption that the image intensities are statistically homogeneous for each region. That model detect inward contours starting with one initial curve that can be anywhere in the image.

A model that draws on intensity information in local regions was also proposed by *Li et al* [30]. First, they define a region-scalable fitting energy functional in terms of a contour and two fitting functions that locally approximate the image intensities on the two sides of the contour. The minimization of the energy is achieved by minimizing the integral over the points in the image, and then smoothing the contour by penalizing its length. Note that $| \bigtriangledown \phi|$ is again replaced by the smoothed Dirac function. The equation is written as:

$$\frac{\partial \phi}{\partial t} = \delta(\phi)[\nu(div(\frac{\bigtriangledown \phi}{| \bigtriangledown \phi|})) - (\lambda_1 e_1 - \lambda_2 e_2) + \mu(\bigtriangledown^2 \phi - div(\frac{\bigtriangledown \phi}{| \bigtriangledown \phi|}))] \tag{4.5}$$

The term $\nu(div(\frac{\bigtriangledown \phi}{|\bigtriangledown \phi|}))$ has a smoothing effect and is fundamental to maintain a regularized contour. The data fitting term $(\lambda_1 e_1 - \lambda_2 e_2)$ is responsible for driving the contour toward the object boundary. The last term, called level set regularization term searches for the regularity of the function. The function is initialized with a negative constant value inside a region and a positive constant value outside. The authors justify that choice saying

that the evolution is significantly faster than using the initial function as a signed distance map. They also affirmed that their method is much simpler and more efficient than the piecewise smooth model [29] in terms of the computational time and accuracy.

4.2.3 Hybrid

In order to improve the segmentation performance, the integration of edge and region based information using active contours has been proposed by a few authors. Geodesic active region is a supervised active contour model, proposed by *Paragios et al* [31] [32], integrating edge and region-based segmentation modules in an energy function. *Zhang et al* [33] also applied that combination to achieve robust and accurate segmentation results using the following equation:

$$\frac{\partial \phi}{\partial t} = \mid \bigtriangledown \phi \mid [\alpha(I - \mu) + \beta(div(P\frac{\bigtriangledown \phi}{\mid \bigtriangledown \phi \mid}))] \tag{4.6}$$

The speed term F integrates both boundary and region information. The first term encourages the contour to enclose the regions with gray-levels greater than a specific value. The second term aids the contour to attach areas with high image gradients. They tried to solve the problem from a more geometric perspective, evaluating the advantages of the model over the region based model proposed in [29]. The proposed model has been extended to *3D* images, to solve segmentation problems on volumetric medical data.

4.2.4 Shape *Priors*

Ultrasound B-scans suffer from poor contrast and frequently is observed absence of boundary segments. To overcome these problems, some authors introduced *a prior* shape knowledge on the level set framework, which need an off-line training process to learn the specific characteristics of the object shapes:

- The *prior* shape used by *Paragios* [32] is expressed by a probabilistic level set distance map, which is composed by a set of training examples. The global shape correspondence is determined through registration and the *prior* knowledge is established by encoding pixel-wise stochastic level set. This method can detect single objects with complex topology but is unable to recover structures from connected topologies.

- *Bernard et al* [34] used the Generalized Gaussian as *a priori* distribution. The proposed level set model is driven by the statistics of a radiofrequency signal modeled through the mentioned *prior* distribution. They used radial basis functions and multiphase level set functions to detect more than one ROI.

- *Oktay* and *Akgul* [35] went further by implementing global and local *priors*. The shape-based global *prior* is incorporated by regularly reinitializing the level set surface under the influence of the physician detected contours, and the local *priors* with image and temporal information are learned through boosting (training and classification approach). The separately trained inner and outer heart wall information can then be used in the segmentation by level set to eliminate any ambiguity between endocardium and epicardium.

4.3 Watershed

The watershed algorithm was also widely and successfully applied in the medical ultrasound domain as a powerful segmentation tool. It is based on the assumption that the gradient magnitude of the image is a topographic surface. The gradient local minimum of each region is like a valley from which the water will rise up. The position where each two valleys are converging gives rise to a boundary called a watershed line. Each local minimum is then surrounded by the watershed line, which represents a segmented region. This methodology is widely used in addition with pre and post-processing techniques, to segment echocardiographic images:

- *Cheng et al* [36] combine the advantages of the watershed methodology with those of active contours (watersnakes). The method uses watershed to pre-segment the image, which expedites boundary detection and generates the initial position of the snake. The active contour evolves then to determine a first left ventricle boundary for posterior tracking of its boundaries, in a sequence of echocardiographic images as shown in Figure 4.7.

- *Deka* and *Ghosh* [37] proposed a segmentation model having four stages. It starts with the pre-processing stage that consists of applying a histogram equalization method and a filtering, using an adaptive median filter to reduce the effect of the speckle noise. In the second stage,

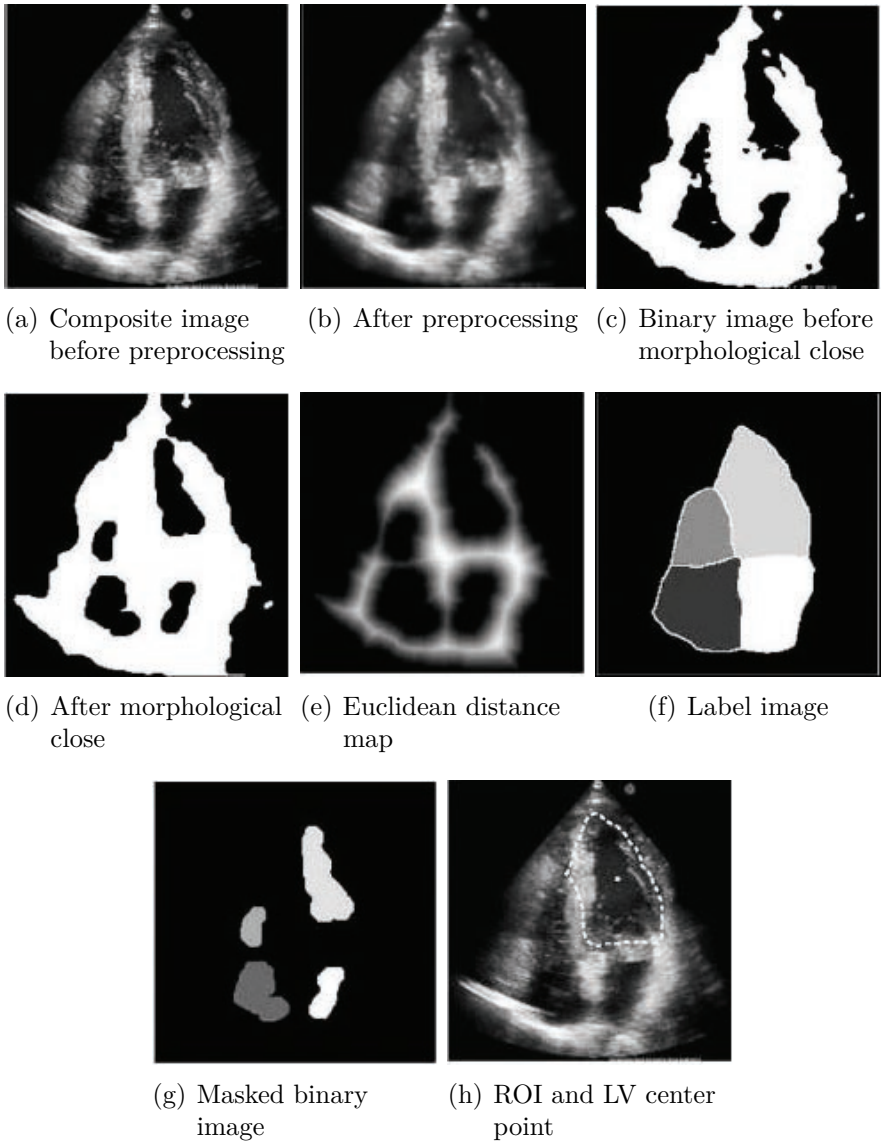

(a) Composite image before preprocessing (b) After preprocessing (c) Binary image before morphological close

(d) After morphological close (e) Euclidean distance map (f) Label image

(g) Masked binary image (h) ROI and LV center point

Figure 4.7: ROI segmentation using the Watersnake method [36].

a gradient map suitable for watershed segmentation using a multiscale morphological gradient is produced. This gradient image is then thresholded before applying the watershed transformation, to reduce the over segmentation problem. After the watershed segmentation procedure, similar neighboring regions are merged considering a global threshold. This model was compared with the classical watershed segmentation using echocardiographic images. It was then concluded that the proposed

pre-processing and post-processing techniques perform better than the classical existing method.

- *Lacerda et al* [38] used a semi-automatic method to extract the left ventricle internal border using classical image processing techniques combined with radial search. The first step of the preprocessing phase uses high boost filtering, then elevation filter, and a LoG filter to make the region more uniform. The watershed algorithm is first used to identify and label regions in the pre-processed image and then small regions are eliminated. For the long-axis images segmentation (where the segmentation errors are more common), the information from sequential frames is used to select points that are candidates for the left ventricle boundary (Figure 4.8).

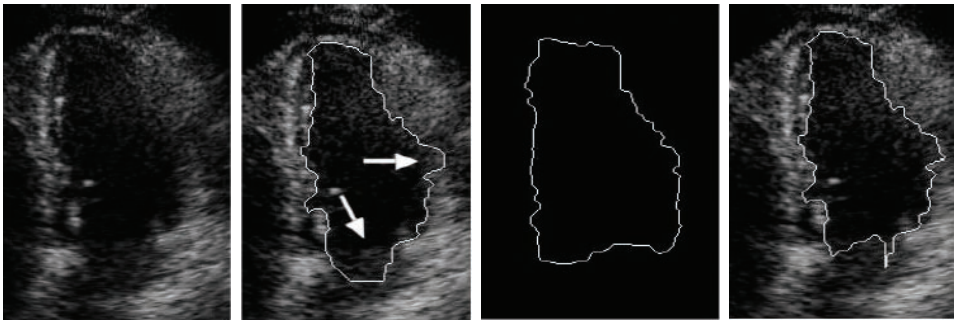

(a) The original image

(b) Segmentation errors in the current frame

(c) Segmentation from a previous frame, used as reference

(d) Result after sequential radial segmentation

Figure 4.8: Representative results from the proposed sequential radial search algorithm of *Lacerda et al* [38].

- An improved segmentation by watershed is proposed by *Li* [39] that is based on a merging scheme, which takes into account comprehensive consideration of gray scale information, edge information, and the relationship between neighboring regions. The results are accurate contours and the over-segmentation phenomenon available in the traditional watershed segmentation is prevented.

4.4 Limitations

As exposed previously, there are several methods that attempt to segment the left ventricle as the most important examined heart cavity. Reliable performance, however, is only provided by algorithms that use *a priori* knowledge and semi-automatic algorithms.

Despite of the promising results of the reviewed fully automatic methods, most of them have little success outside the research environment due to the many artifacts present in the *2D* echocardiographic data. Thus, none of them is capable of producing a reliable contour extraction to be applied in the clinical practice. The low contrast and dropouts on the boundaries are the largest error sources of those algorithms, leading the automatic border detection to fail. The difficulties are also related to the characteristic speckle noise, the existence of papillary muscles, valve and vein structures. The selection of the cavity boundaries is only possible with the interaction of trained experts.

The literature in left ventricle segmentation algorithms is vast; however the automatic segmentation of the four heart chambers is a more complex task and less studied. Nevertheless, reliable segmentation of the whole heart continues a great research field due to its importance to achieve a fully automatic segmentation tool.

Chapter 5

Echocardiographic Segmentation Methodology

In order to extract reliable contours, an automatic segmentation method is proposed, capable to accurately extract the heart cavity boundaries. The first step consists in the detection of low-level feature in the echocardiographic image. It corresponds to the points where there is a specific order in the frequency domain, using the phase symmetry approach proposed by *Kovesi* [40]. Then, the level set segmentation method is applied to extract the boundaries. Morphological operations are needed to eliminate small regions and to smooth the contours. In the following sections, the proposed segmentation method for the simultaneous heart cavities segmentation is described.

5.1 Pre-Processing

Various filtering techniques were tested in a preliminary phase on the noisy echocardiographic B-mode images; the median filter, for example, was applied on the image (space domain). With this filter each pixel is replaced by a non-linear combination of the pixel values in the neighborhood, being a good salt and pepper noise attenuator. The choice of this filter was due to the similarity of the typical speckle noise of ultrasound images with the salt and pepper noise. An example of another filter tested, applied in the

frequency domain was the anisotropic diffusion. It is an iterative filter that suppresses noise while preserving the edges of the image. However, none of them have demonstrated a significant diminution of the available noise.

Observing the structures of the heart it is visible that the features of interest, the heart boundaries, have a characteristic form. The problem to segment it is that the boundaries have not the same pixel intensities, having in some cases a poor defined edge. Due to these characteristics, a technique that is invariant to changes in image brightness or contrast was applied, the phase symmetry.

5.2 Phase Symmetry

Due to the importance of this noise reduction method for the following steps, it is not considered as a pre-processing method but the first step of the segmentation process.

Any discrete signal can be represented by its correspondent discrete fourier transform (DFT), the sine and cosine functions with specific amplitudes, giving rise to a set of scaled waves in the time domain that synthesizes the original signal.

Phase congruency is a low-level feature detector, derived from the Fourier analysis. In [41], *Morrone* and *Owens* give a general definition about features based on the phase analysis. These features occur at points of maximum phase congruency, and using the value of the phase it is possible to determine the type of feature.

The points detected by the phase congruency are significant if they occur over a wide range of frequencies. For example, at the points of an edge transition all the Fourier components are exactly in phase. For all other points the phase of the sinusoidal components vary, resulting in a low phase congruency, see Figure 5.1. All the Fourier components that form the square wave in the step edge point are in phase. The phase is 0° or 180° depending whether the step is upward or downward. In all the other points the phase of each sinusoidal component vary, resulting in a low phase congruency. This is an example how features can be detected and described depending on the phase.

In order to compute the local phase and estimate the phase congruency from a signal, *Kovesi* [40] used Log-Gabor wavelets. A log Gabor filter is constructed in the frequency domain and has a transfer function on the

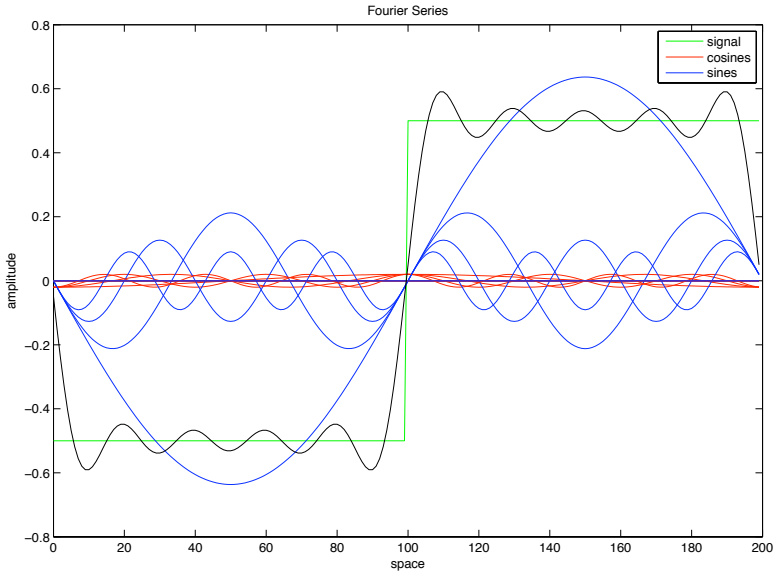

Figure 5.1: Fourier Serie of an edge step presenting a high phase congruency. Just the first 32 Fourier components are shown. The black signal is the synthesized signal using this 32 components.

linear frequency scale given by:

$$LogG[f] = \exp^{\frac{-(log(f/f_c))^2}{2(log(\kappa_\beta))}} \tag{5.1}$$

where f_c is the center frequency and $0 < \kappa_\beta < 1$ (*Kovesi* calls this parameter $sigmaOnf$) is related to the bandwidth β [42]:

$$\beta = -\frac{2\sqrt{2}}{\sqrt{\ln 2}} \ln \kappa_\beta \tag{5.2}$$

Figure 5.2 illustrates how the filter shape change when κ_β is changed while maintaining the center frequency f_c constant. When κ_β increases, the ratio of filter cycles (number of modes) increase too.

When selecting the filter parameters, care must be taken to avoid aliasing [42]. Aliasing happens when the long filter tails run beyond the *Nyquist* limit of $f = \frac{f_s}{2} = 0.5$. *Boukerrroui et al* in [42] give the following condition to

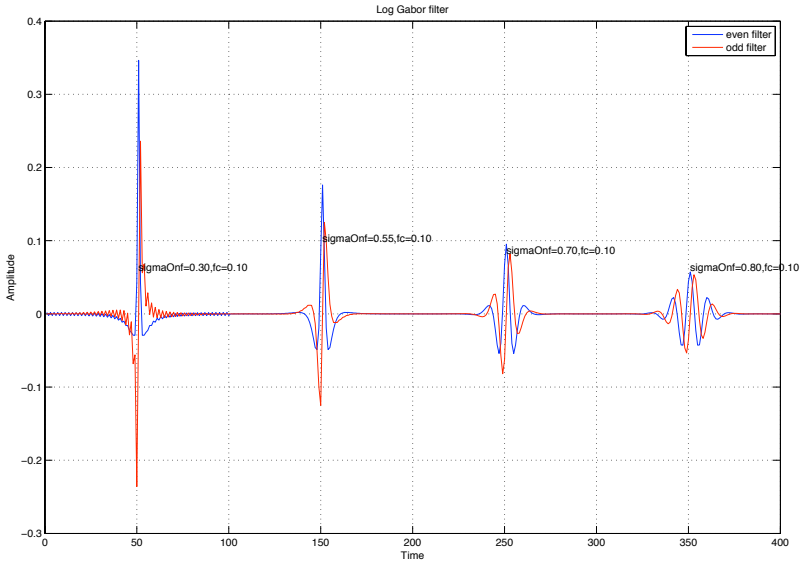

(a) Log Gabor wavelets in the time/space domain

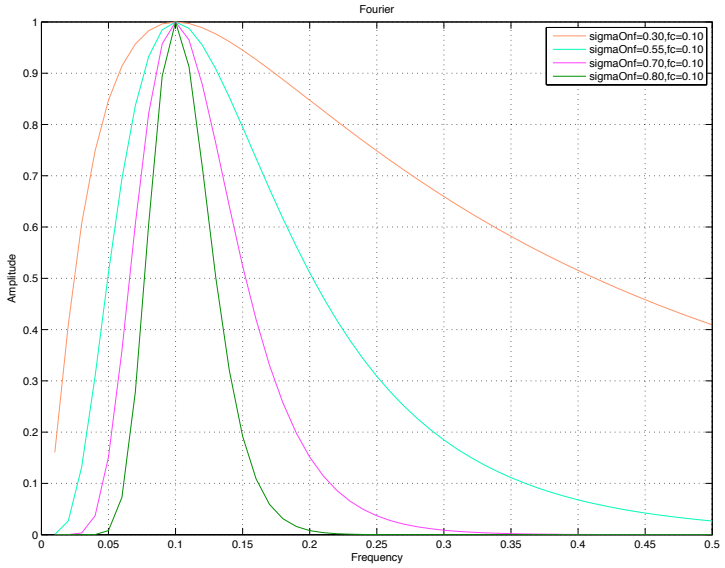

(b) Log Gabor wavelets pair in the frequency domain

Figure 5.2: Gabor wavelets with increasing tuning frequency (fc) and constant shape ratio κ_β ($sigmaOnf$).

avoid aliasing:

$$f_c < \frac{\kappa_\beta^n}{2}. \tag{5.3}$$

where n controls the frequency limit.

Inspired by the properties of the Phase Congruency, *Kovesi* shows also how symmetries in image intensity values give rise to special phase patterns. Any symmetry in a signal implies some type of periodicity. Intuitively, periodicity should be easier to analyze in the frequency domain then in the time domain, as it can be seen in Figure 5.3. All Fourier series at points of symmetry are either at minima or at maxima of their cycles. At this points, the Fourier series components are at the most symmetric points. In the same way, at anti-symmetry points in the signal, the Fourier series are at the most anti-symmetric points in their cycles. *Kovesi* has adapted the phase congruency measure to the detection of symmetry and anti-symmetry. The symmetry measure is defined as:

$$\begin{aligned} Sym[n] &= \frac{\sum_s \lfloor A_s[n][\mid \cos(\phi_s[n]) \mid - \mid \sin(\phi_s[n] \mid] - T \rfloor}{\sum_s A_s[n] + \epsilon} \\ &= \frac{\sum_s \lfloor [\mid e_s[n] \mid - \mid o_s[n] \mid] - T \rfloor}{\sum_s A_s[n] + \epsilon} \end{aligned} \tag{5.4}$$

and the anti-symmetry measure is given by:

$$AntiSym[n] = \frac{\sum_s \lfloor [\mid o_s[n] \mid - \mid e_s[n] \mid] - T \rfloor}{\sum_s A_s[n] + \epsilon} \tag{5.5}$$

where $e_s[n]$ is the even symmetric part and $o_s[n]$ is the odd symmetric part of the filter at scale s. The $\sum_s$ joins implicitly the information of the various filters at different scales. At a point of symmetry the absolute value of e_s will be large and the absolute value of o_s will be small. At points of anti-symmetry, the response is reversed and as a consequence the odd part of the filter will have a large response while the absolute value of e_s is small. $A_s[n]$ is the magnitude of the filter response at a given wavelet scale, the term ϵ is a small constant to prevent division by zero in the case where the signal is uniform and no filter response is obtained, and the factor T is a noise compensation term.

Extension to *2D* images is made by applying the *1D* analysis over several orientations and combining the results to provide a single measuring of

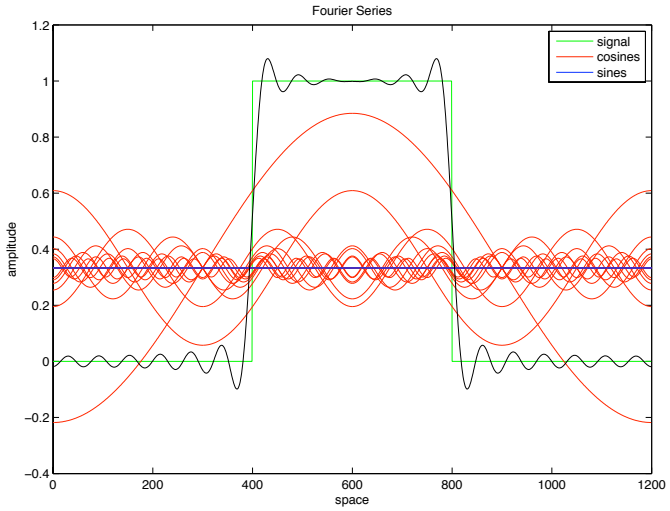

(a) Square wave

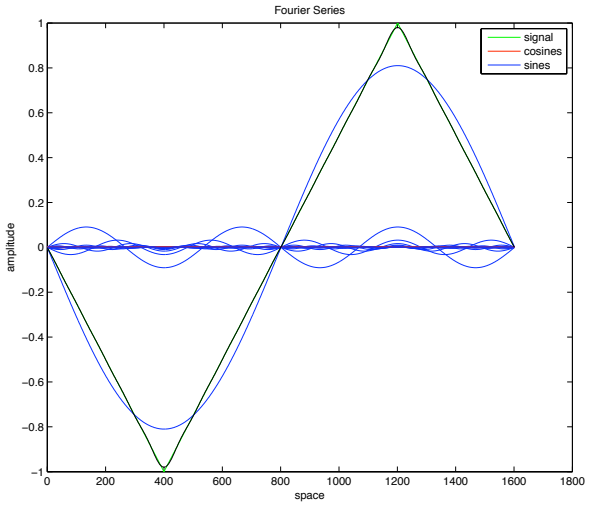

(b) Triangular wave

Figure 5.3: The Fourier component are all at the most symmetric points in their cycles at symmetric points, and are at the most anti-symmetric points at anti-symmetry points.

the feature significance. The *1D* symmetry measure just explained was applied along six orientations and the results of each orientation combined in a weighted sum. An example of the phase symmetry image obtained using this approach is shown in Figure 5.4.

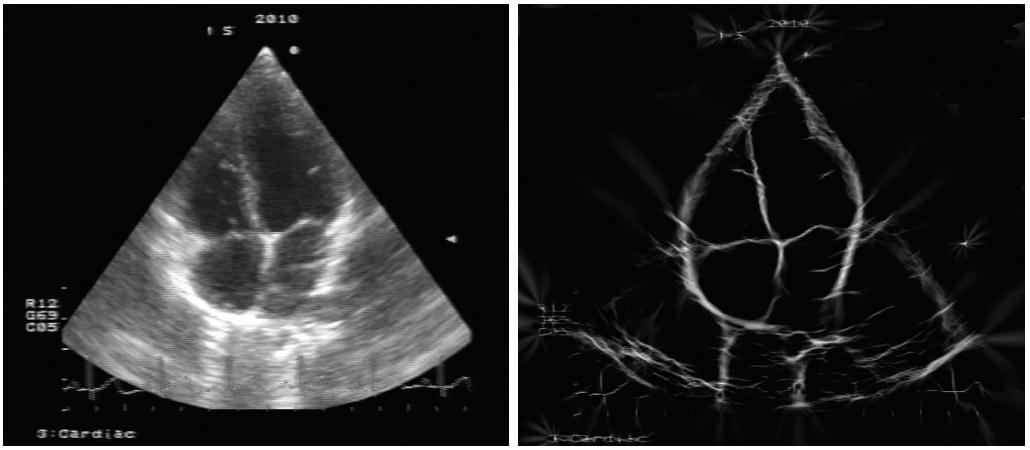

(a) An original echocardiographic image (b) Output of the phase symmetry

Figure 5.4: First step of the proposed method.

5.3 Boundary Detection

Active contour models show very good results and flexibility in the segmentation of ultrasound images. An implicitly formulation of this methodology (level set) was chosen for the segmentation of the four heart cavities. The advantages that justify the choice of the methodology are:

- Non-parametric representation of the evolving object boundary
- Detection of more than one boundary simultaneously
- Geometrical flexibility
- Production of closed boundaries, always
- Simple extension to *3D*

The different curve evolution models presented in section 4.2.4, namely the classical edge-based, the model proposed by *Chan*, the *Li*'s region scalable

fitting and the hybrid model of *Zhang*, were implemented and tested on synthetic images and on real echocardiographic B-mode frames, pre-processed with the phase symmetry algorithm. Each method was studied in terms of its complexity, curve evolution and accuracy in the detection of the cavities. The evaluation (presented in the next chapter) led us to conclude that additional terms for the velocity function F, appearing in the region-based and hybrid equations do not produce improvements compared to the performance of the edge-based formulation.

Thus, the model followed in this work was the edge based formulation:

$$\frac{\partial \phi}{\partial t} = \mid \bigtriangledown \phi \mid [k_0 div(\frac{\bigtriangledown \phi}{\mid \bigtriangledown \phi \mid}) + \nu] P \tag{5.6}$$

In order to perform the curve evolution, ϕ is initialized as a signed distance function in the Euclidean space, defined as follows: the central pixel of the mask image has the largest value and decrease at each neighbor element, ending with a zero value at the four corners of the image. This initialization increases the stability and the curve evolution quality. A representation of the signed distance function is illustrated in Figure 5.5.

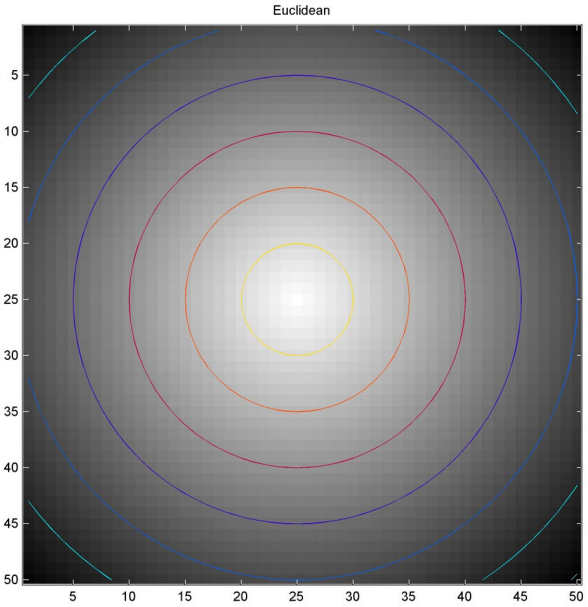

Figure 5.5: The initial mask, a signed distance function in the Euclidean space.

The function ϕ is iteratively modified according to the vector field of the image gradient $\mid \bigtriangledown \phi \mid$ and the mean curvature term $K(\phi(x,y)) = div(\frac{\bigtriangledown \phi}{\mid \bigtriangledown \phi \mid})$,

given by:

$$K(\phi(x,y)) = \frac{\phi_{xx}\phi_y^2 - 2\phi_x\phi_y\phi_{xy} + \phi_{yy}\phi_x^2}{(\phi_x^2 + \phi_y^2)^{3/2}} \tag{5.7}$$

where ϕ_x and ϕ_{xx} denote respectively the first and second order partial derivatives of $\phi(x,y)$ regarding to x, and ϕ_y and ϕ_{yy} denote the same regarding to y. The function evolves at least in the regions where ϕ is smooth and $\bigtriangledown\phi$ does not vanish, controlling the regularity of the curve that moves in the normal direction with speed $[k_0 div(\frac{\bigtriangledown\phi}{|\bigtriangledown\phi|}) + \nu]P$. The constant value k_0 looks for the equilibrium between the regularity and robustness of the contour evolution and the constant value ν is a correction term, to ensure that the terms $[k_0 div(\frac{\bigtriangledown\phi}{|\bigtriangledown\phi|}) + \nu]$ remain always positive. It can be interpreted as a force that provides a quicker convergence, expanding or shrinking the curve.

As mentioned in the previous chapter, the classical stopping function P presents some drawbacks due to its gaussian dependence. Alternative stopping functions were analyzed, having the logarithmic dependent function [43] shown the better performance in stopping on the edges (where its numerical value vanishes):

$$P = log(|\frac{I-a}{\gamma}| + 1) \tag{5.8}$$

where I is the image, a is the average intensity value of the image, and γ is the dynamic range of the region being analyzed. For low $|I-a|$ values the level set is nearby the region to be segmented reducing its evolution speed (low P) for the ROI detection. For high $|I-a|$ values the level set is far away from the region to be segmented, and then the evolution speed remains high and almost constant. An important advantage of using this stopping function is the capability of the level set to adjust itself to the low intensity regions.

The function ϕ is updated at each time interval:

$$\phi^{t+1} = \phi^t + \triangle t\frac{\partial\phi}{\partial t} \tag{5.9}$$

suffering shrinking or expansion iterations until the functional has converged to the boundary (see Figure 5.6). The closed curve will produce surfaces with zero value ($\phi = 0$) on the boundaries, positive for pixels inside the curve ($\phi > 0$) and negative for pixels outside the curve ($\phi < 0$).

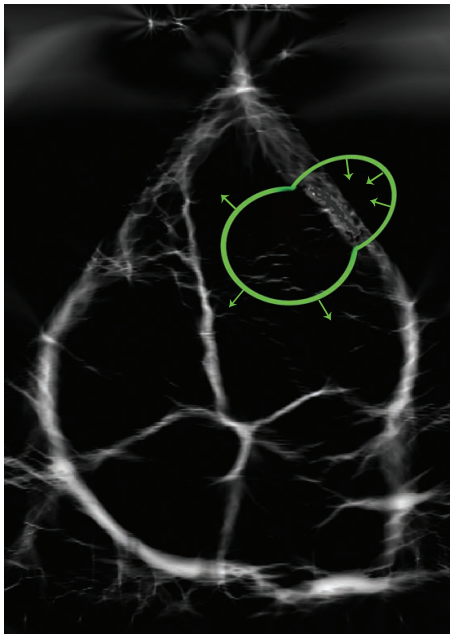

Figure 5.6: Level Set curve propagation.

5.4 Morphological Operations

Due to the echocardiographic image characteristics and the level set nature, several small noisy regions are also detected (see Figure 5.7(a)) and should be eliminated to put in evidence only the four cardiac cavities. Since the output of the segmentation is a binary image, the following procedure was carried out. First, in order to detect each contour, an initial pixel is selected for one contour, and then one proceeds through its adjacent pixels until the starting pixel is reached again. In this way, all pixels that form the contour are identified. This procedure is repeated for each contour and the respective area is computed. The contours corresponding to the four biggest areas are the heart chambers (Figure 5.7(b)). As a final step, the irregularities in the four detected contours are smoothed using dilation and erosion morphological operations (Figure 5.7(c)).

5.5 Similarity Metrics

In the medical domain, it is mandatory to evaluate rigorously the methods before they can be accepted and used in the real clinical practice. In order to evaluate our method and to propose it to a real clinical environment, we have

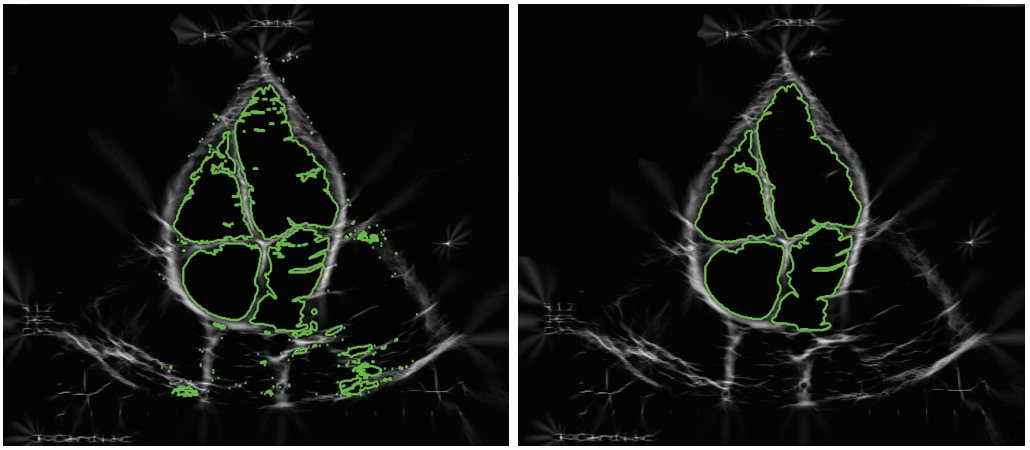

(a) Output of the proposed level set

(b) After discarding small regions

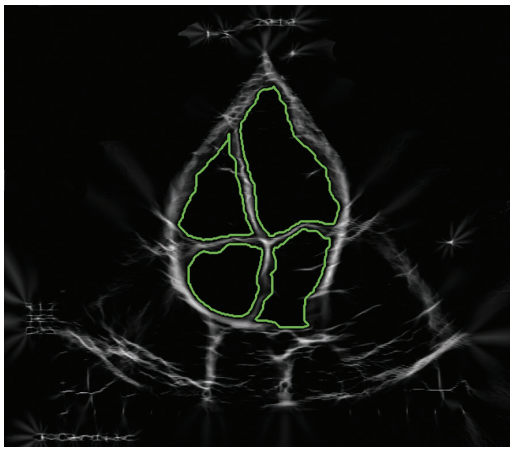

(c) After smoothing with morphological operations

Figure 5.7: Steps from the level set evolution to the final output.

done exhaustive comparisons against the manual boundary labels drawn by physicians[1] (Figure 5.8).

There are different approaches to compare two contours [44]. The most used approaches are based on the local distances between the two contours or on the evaluation of the regions common to the regions circumscribed by both. For each approach, two similar metrics were used. The Pratt function and the mean distance error as contour based metrics, the similarity angle and the similarity region for the region based approach.

[1]The references used for the evaluation of the automatic algorithm are contours drawn by a trained expert.

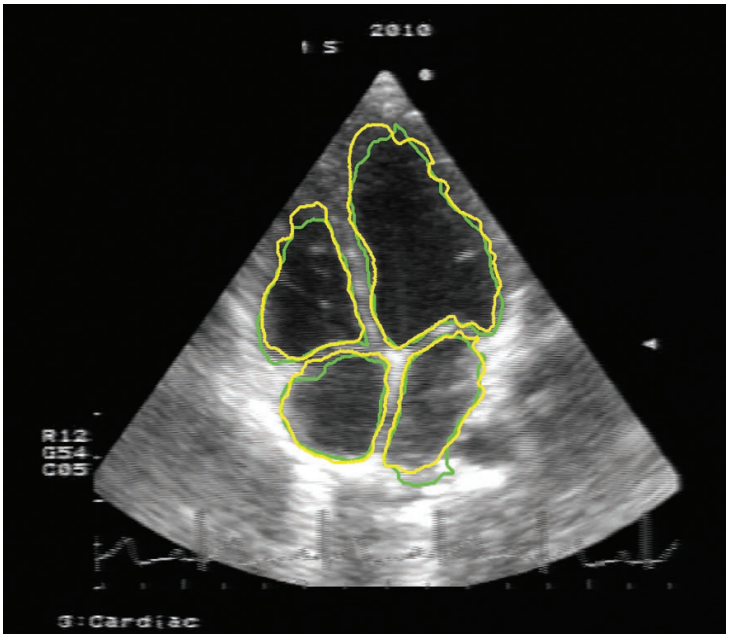

Figure 5.8: Contour produced by the algorithm overlapped on the manual drawn by the physician.

5.5.1 Contour Based

This approach starts with the detection of the mean contour that is a line equidistant to both contours under analysis, computed after overlapping both contours. In the regions where the contours coincide, the mean contour also coincide. In the regions where the contours do not agree exactly, a line is defined with the same distance apart from the contours (see Figure 5.9(a)). Each point in this mean contour is identified and a perpendicular line is traced through it that will intersect the two contours under analysis; the two points (one on each contour) where this interception occurs, are called corresponding points (see Figure 5.9(b)). A distance d_i is defined, as the distance between corresponding points and the similarity evaluation is based on these values. We used two similarity metrics based on d_i.

5.5.1.1 Pratt Function

The Pratt function (PF) is a non linear metric [45] that characterize the global behavior of the discrepancies between the comparing contours, which is given by:

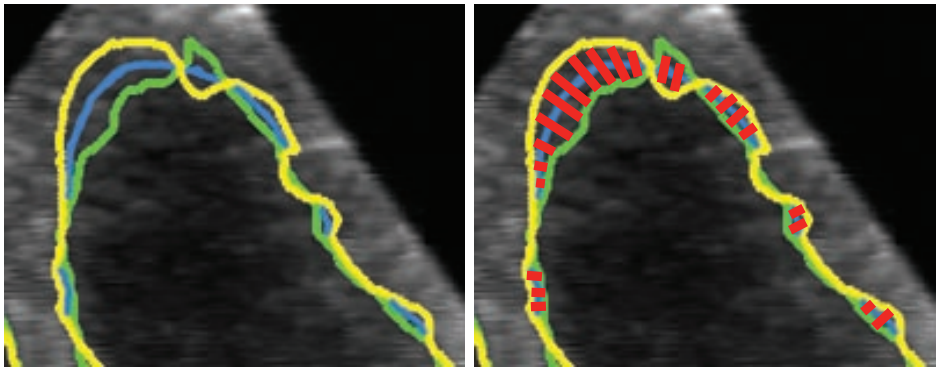

(a) Mean contour (blue)

(b) Mean contour and corresponding points (red)

Figure 5.9: Example of the contour based evaluation.

$$PF = (\frac{1}{N})\sum_{i=1}^{N}(\frac{1}{1+Q\times d_i^2}) \tag{5.10}$$

The Pratt index varies between 0 and 1, where 1 is the exact overlapping of the two contours. The term N is the number of corresponding points. The normalization parameter Q is related to the contour size, having a value such that $PF = 0.5$ when all the distances are equal to 3 pixels.

5.5.1.2 Mean Distance Error

This metric gives an average view of the distances between contours and is defined as:

$$MDE = \frac{1}{N}\sum_{i=1}^{N} d_i \tag{5.11}$$

The larger is the MDE value, the higher is the dissimilarity between the compared contours.

5.5.2 Region Based

The interior of the two contours to be compared is filled as shown in Figure 5.10. The two resulting binary images are overlapped and the comparison will be based on the morphological similarity [46]. The metrics used based

on this approach are the similarity angle and the similarity region described below.

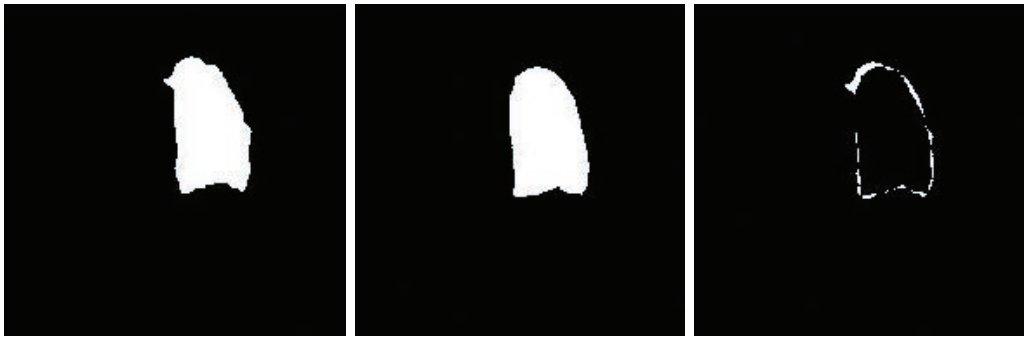

(a) Produced by the proposed segmentation method

(b) Drawn by the expert physician

(c) Mismatch pixels for the compared images

Figure 5.10: White filled contour of the left ventricle.

5.5.2.1 Similarity Angle

The similarity angle (SA) is a measure of the morphological similarity of two contours. Two vectors H and I are defined, where each vector is the linearization of each image. If one image has n $\times$ m pixels, the linearization vector will be a 1D vector with m $\times$ n pixels. These two vectors can be considered elements of a Hilbert space, where the similarity angle denotes the angle between the two binary image vectors H and I. Using the definitions of the Euclidean inner product we defined the Similarity Angle as:

$$SA = \arccos\left(\frac{\overrightarrow{H} \cdot \overrightarrow{I}}{||\overrightarrow{H}|| ||\overrightarrow{I}||}\right) \tag{5.12}$$

The angle varies between 0° and 90° for two similar and dissimilar contours, respectively.

5.5.2.2 Similarity Region

A similarity measure can be obtained based on the uncommon area (pixels) of the overlapped regions:

$$SR = 2 \times \left(\frac{A \times B}{A + B}\right) \tag{5.13}$$

where A is the filled interior of the contour obtained by the algortihm and B the filled interior of the contour drawn by the physician. SR is the ratio between uncommon regions $A \times B$ and the sum of both regions, multiplied by a normalization factor.

Chapter 6

Results

The contours obtained by the proposed segmentation method were compared with those ones manually drawn by physicians, using the similarity metrics described in the previous chapter. The performance was also compared with the level set models proposed by *Chan* and *Vese*, *Li et al*, *Zhang et al*, and with the watershed technique explained in section 4.3, having as reference the contours manually drawn by the expert physicians. Before applying these methods, the images were also pre-treated with the phase symmetry algorithm.

The boundaries extraction is an automatic process without any user intervention, and convergence is achieved after a few iterations. Figure 6.1 shows some results, illustrating the reference contours drawn by the expert in yellow and contours resultant from applying the proposed method in green.

In the following, it is presented the evaluation concerning to the capability of each method to extract simultaneously the four cardiac cavities. The comparison between methods is made using the *Matlab* implementation of the one-way ANOVA, where each algorithm (column) represents an independent sample containing mutually independent observations. The results are graphically displayed using boxplots of the data that are useful to visualize the median and variance of the distributions.

6.1 Data Set

The data base consists of four-chamber images randomly extracted from echocardiographic videos collected by two different ultrasound equipments:

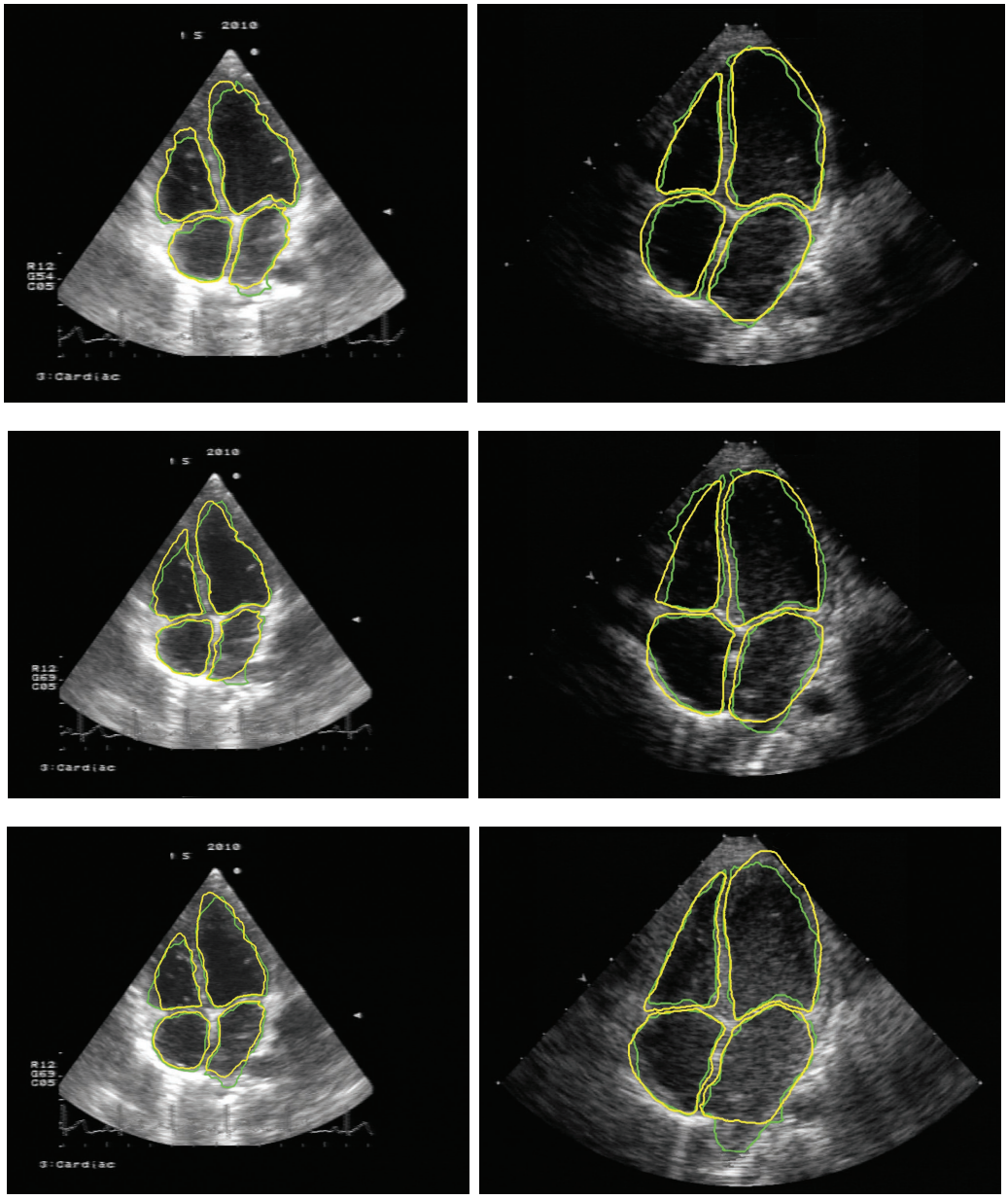

Figure 6.1: Examples of contours obtained using the proposed method (green) overlapped with contours manually drawn by physicians (yellow). The images on the left are from an echocardiographic equipment and the images on the right are from another standard equipment.

Acuson Sequoia 512 and Aloka SSD 2200. The videos correspond to four children (two children from each equipment). Only frames with the four

heart cavities visible and in systole were selected. Tests were accomplished taking into account six frames from each child, in a total of twenty-four images of 576 $\times$ 720 pixels.

6.2 Performance Analysis

The analysis on each box provides a fast visual examination of the median value, the 75th percentile at the upper edge (hinge) of the box and the lower hinge at the 25th percentile. The whiskers extend to the most extreme data points, minimum and maximum data value, except when outliers are detected. The outliers are plotted individually, as any point that is above the 75th percentile by 1.5 times the inter-quartile interval (similarly below the 25th percentile). The first quartile goes from minimum to the 25th percentile, the second quartile goes from 25th percentile to the median value, the third quartile goes from the median value to the 75th percentile, the fourth quartile from 75th percentile to the maximum value and the middle two quartiles (from 25th percentile to the 75th percentile) is the inter-quartile range (IQR). An example of the graphical display method is shown in Figure 6.2.

From the 24 random selected images only the ones in which it was possible to automatically segment the four heart cavities were analyzed statistically, i.e. those ones in which it was obtained four closed contours. That analysis was possible on 23 images using the proposed method, on 20 images using the Watershed technique, on 19 images with the hybrid algorithm proposed by Zhang (equation 4.6), on 14 images using Li's region based scalable fitting method (equation 4.5) and only on 7 images with Chan's active contour (equation 4.4).

We performed three different sets of evolutions, consisting in:

- The five segmentation algorithms (Proposed method, Chan, Li, Zhang, Watershed)
- The three algorithms with better performance (Proposed method, Zhang, Watershed)
- The proposed method

In order to compare the different algorithms among them, only the segmented images commonly to all methods might be used; to compare the five methods were used the 7 common images, to compare the three methods with better performance were used the 19 common images, and to evaluate

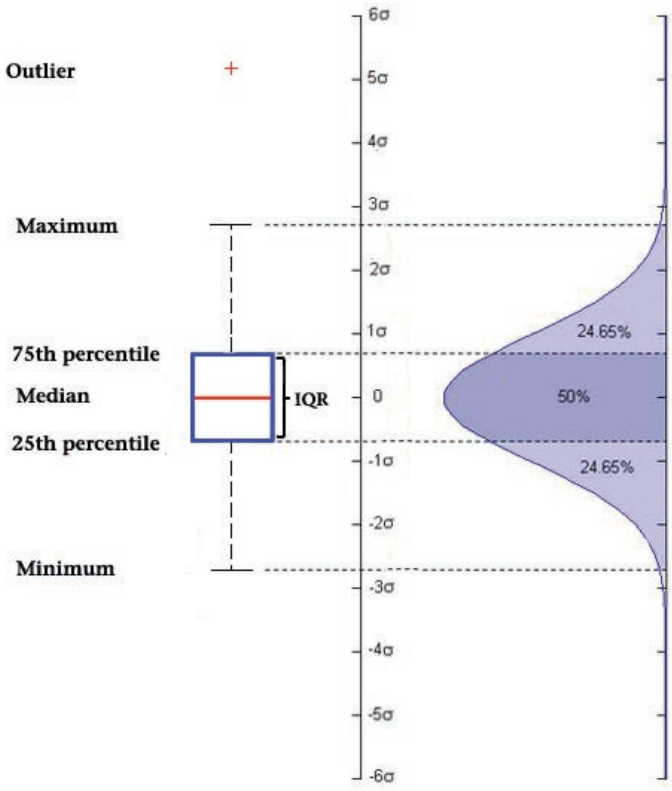

Figure 6.2: The boxplot evaluation.

the proposed method we used the 23 images that the algorithm was able to segment.

6.2.1 Preliminary Assessments

Using the 7 images that all methods were able to segment, we constructed the boxplot graphic shown in Figures 6.3 and 6.4. The Pratt function explained in section 5.5.1.1 was used, which varies in the range 0 to 1, being 1 the case of the perfect contour overlapping. With this metric we are comparing 28 contours (7 images; four contours each image). The similarity region (section 5.5.2.2) varies in the same range as the Pratt function (0 to 1) and with this metric we compared the performance of the five algorithms in each cavity separately.

Using the Pratt function as analysis metric, the closer the values are to 1 the better performance is available. Observing the maximum value of each boxplot in Figure 6.3 (discarding the outliers), the region based models from

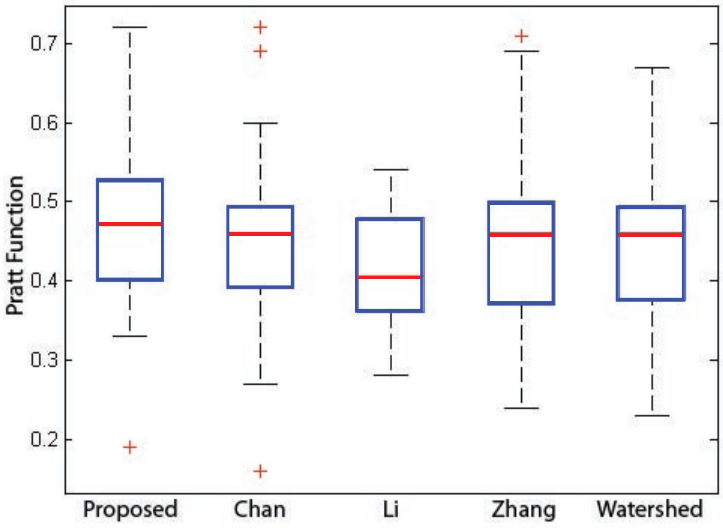

Figure 6.3: Boxplots - Pratt function of the five segmentation methods using 28 contours (7 images).

Chan and Li have the lowest maximum values, meaning worst performance. The median values for the proposed, Chan, Li, Zhang and watershed methods are respectively: 0.47; 0.46; 0.41; 0.46 and 0.46. The highest value (best performance) is achieved for the proposed method while the region scalable fitting model from *Li et al* shows the worst median value. The Zhang and the Watershed methods have the largest second quartile dispersion as well as the entire range (from the minimum to the maximum values). The proposed method has the minor range of the first quartile and with higher values when compared with the alternative segmentation algorithms. The region based level set methods (*Chan* and *Li*) cannot reach the same values for the fourth quartile as the other methods.

The similarity region metric was used to quantify the differences between the output of the tested algorithms and the manual drawn contours for each cavity separately (Figure 6.4). It varies between 0 and 1, where 0 correspond to two contours with none pixels in common and the value 1 to the exact overlapping with the reference contours. This analysis allows the identification of the problematic cavities. From the evaluation we conclude that the right ventricle has the largest discrepancies among segmentation algorithms. The proposed method is the only capable of providing the lower dispersion range and the higher median value, which means better performance. On these

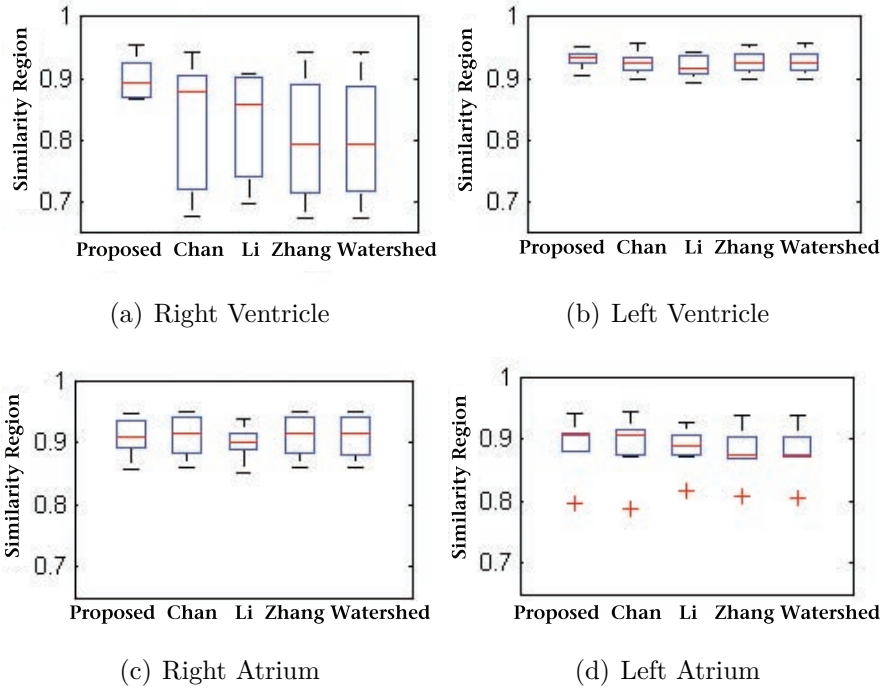

(a) Right Ventricle

(b) Left Ventricle

(c) Right Atrium

(d) Left Atrium

Figure 6.4: Boxplots - similarity region values of the five segmentation methods for each cavity using 7 images.

images, the right ventricle is poor segmented by the other algorithms. The three other heart cavities present similar values on the seven images without significant disagreement between the different segmentation algorithms.

Since the region based methods proposed by Chan and Li are only able to segment 7 and 14 images respectively, and have the worst performance when comparing all methods, they were discarded and the analysis was restricted to the three methodologies with better performance (proposed, Zhang and watershed methods). This procedure has the practical effect of increasing the number of images to 19 (76 contours) to be compared.

The mean distance error was used to compare the 76 contours, as shown in Figure 6.5. The median value of the mean distance error for each algorithm is 4.71; 5.44 and 5.37 for the proposed, zhang and watershed, respectively. Despite these approximate values, the entire range of the proposed method has clearly less dispersion than the entire range of the other two methods. Moreover, the outliers on the proposed method have values near the maximum value in contrast to the ones of the two other methods, which have outliers with large values.

Having increased the number of images, a comparison of each cavity sep-

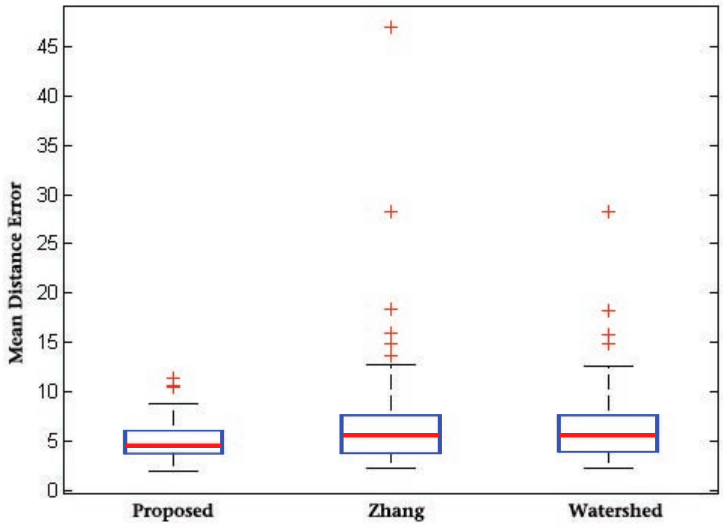

Figure 6.5: Boxplots - mean distance error of the three segmentation methods with better performance using 76 contours (19 images).

arately was made once more, using the similarity angle as metric (Figure 6.6). It is observed again the better performance of the proposed method in comparison with the two other algorithms in segmenting the right ventricle, in terms of median value and inter-quartile range. Observing the entire range of values of each method for this cavity it also shows the better performance of the proposed method. With these additional 12 images, the left atrium has some performance discrepancies, showing the proposed method likewise lower (better) median and inter-quartile values. However, for the two remaining cavities the algorithm has a large range and a high median value (high similarity angle values mean that contours are less similar) having no significant differences comparing with the other segmentation algorithms. Nevertheless, the median value of the proposed method is always lower than the median values of the other algorithms for all cavities.

6.2.2 Global Evaluation of the Proposed Method

The proposed model was able to segment 23 images. Its performance was evaluated considering each heart cavity separately using the mean distance error and the results are shown in figure 6.7.

The median value of the distance error in all cavities is around 5 pixels.

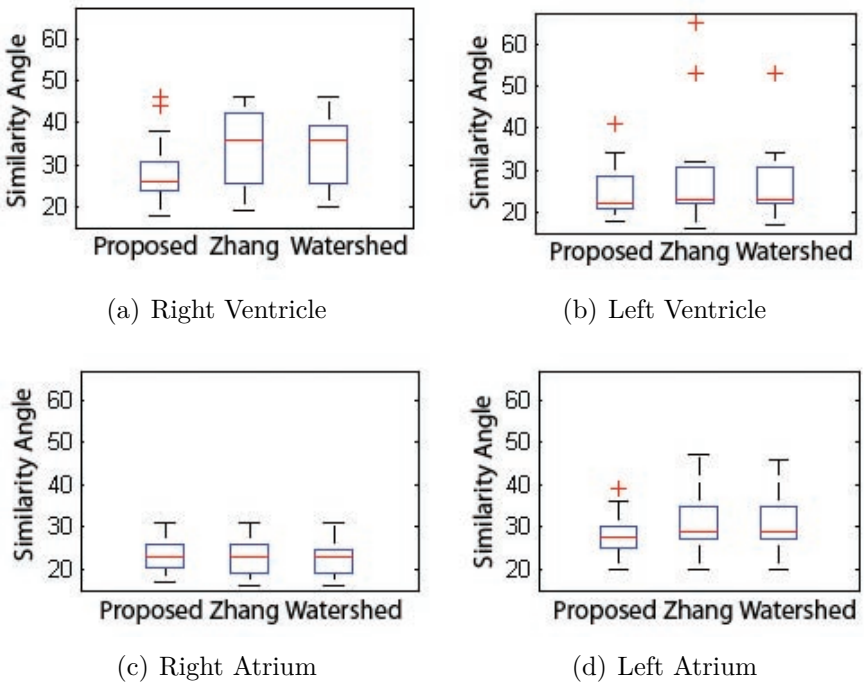

(a) Right Ventricle

(b) Left Ventricle

(c) Right Atrium

(d) Left Atrium

Figure 6.6: Boxplots - similarity angle of the three segmentation methods with better performance, for each cavity using 19 images.

Observing the second and third quartiles as well as the entire range, it is observed better agreement with the reference contours regarding to the right atrium, because it has the lower values. On the contrary, for the already mentioned problematic cavities (right ventricle and left atrium), it is difficult to get a very good segmentation as the large dispersion range of values of the inter-quartile range and entire range demonstrate. This is supported by the two outliers shown in Figure 6.7, which correspond to the images presented in Figure 6.8. The right ventricle's moderator band, described in section 2.1 that is visible in some frames, justifies the incorrect boundary detection by the level set algorithm resulting in the outlier shown in Figure 6.8(a). In Figure 6.8(b), it is shown the imperfect segmentation of the left atrium, highly related to the inter-expert variability, which is briefly discussed in the next section.

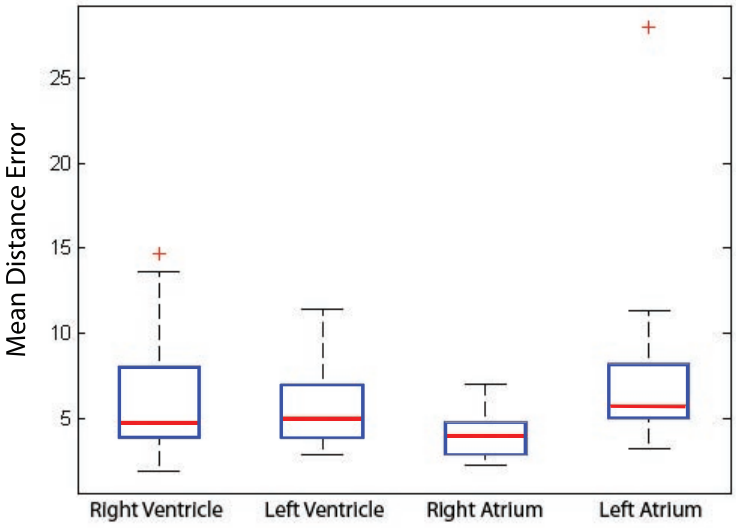

Figure 6.7: Boxplots - mean distance error of the proposed method for each cavity on the 23 images.

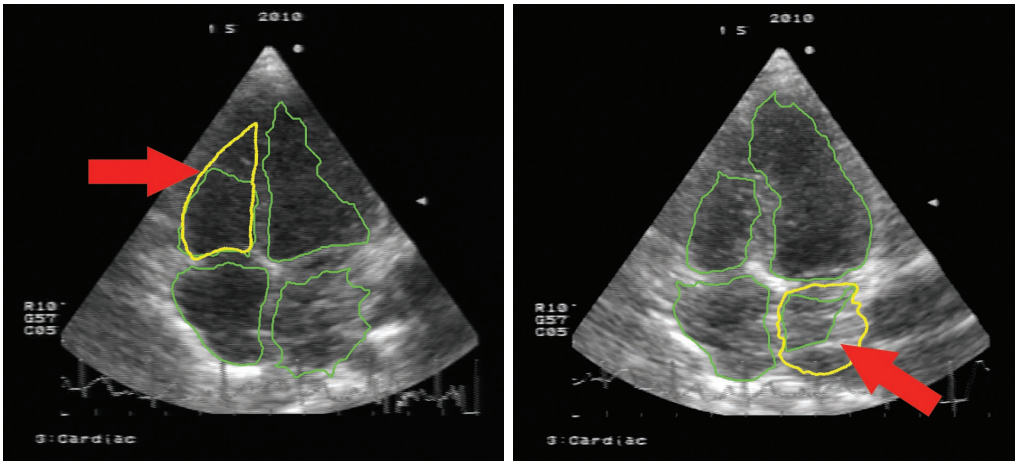

(a) Right ventricle's outlier (b) Left atrium's outlier

Figure 6.8: Worst cases of the proposed segmentation algorithm.

6.3 Limitations of the Evaluation

A good automatic segmentation algorithm should produce accurate contours and comply with clinical realistic contours. However, there exists no

gold standard segmentation for the heart cavities. Several authors address this problem using an average of some manual drawn contours. Nevertheless, this is a hard and time consuming task for the physicians.

In this work, two physicians were asked to manually delineate the contours of the 24 images used (12 images from each one) as reference contours. The evaluation becomes very subjective because it depends strongly on the interpretation given by the physicians about the correct shapes of the cavity contours.

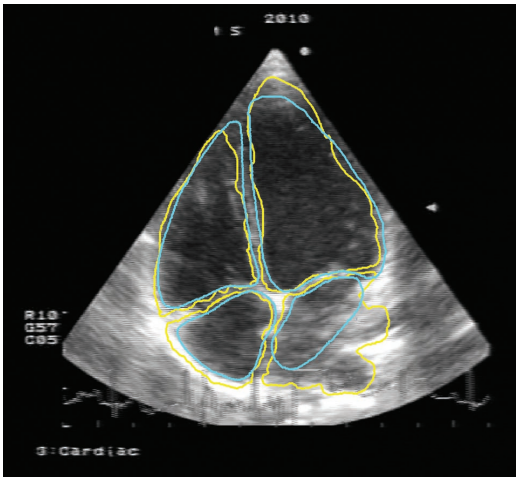

Figure 6.9: Heart cavities delineated by two physicians.

Although the expert contours are considered an unquestionable truth they vary from expert to expert and the errors obtained by the automatic algorithm are in some cases smaller than the ones obtained from two physicians as is the case of the outlier that componds the image in Figure 6.8(b). The segmentation of the left atrium is a complicated task because it is surrounded by pulmonary veins that in most cases hide this heart cavity. Figure 6.9 demonstrates the discrepancy that can arise between two physicians. The first physician (yellow) considered that part of the pulmonary vein belongs to the left atrium, and the result was a rough contour contrasting with the delineation from the second physician (blue), which produced a smooth and regular contour. That demonstrates the importance to have an automatic segmentation algorithm that provides a universal result for a given image in a efficient, fast and easy to use procedure, useful for example in intra-operative monitoring or for the quantification of the heart cavities.

Chapter 7

Conclusions

The method developed in this thesis efficiently segments simultaneously the four heart cavities using echocardiographic B-mode images in an automatic way. The results were far more accurate than the methods proposed until now. The method uses techniques not much researched as is the case of phase symmetry.

The method consists of two steps:

1. The first one highlights the cardiac boundaries, applying for the effect the phase symmetry approach along with six orientations of the image. It is the first time that phase symmetry is used to segment the whole heart cavities, providing substantially noise reduction.

2. The edge based approach has been chosen for the level set evolution, with an improved logarithmic dependent stopping function, which demonstrates better performance than traditional Gaussian or exponential functions.

It was demonstrated that the proposed method is capable to segment automatically and simultaneously the four heart chambers, which is an important advantage when compared with the available methods that only succeeded in trying to segment the left ventricle.

A statistical analysis was made by comparing the proposed method with the three alternative level set algorithms and the watershed methodology. This study was accomplished by confronting the reference contours obtained by experts with the ones provide by the segmentation algorithms applied to 24 images. From the analysis of the comparisons, the results provided by

the proposed method were always superior to the other ones. The positive results obtained with this work acts as motivation to the development of new methods to simultaneously segment the four cardiac chambers, thus assisting image-guided interventions and helping the experts in the clinical diagnosis.

In general, the physicians carry out the heart cavity measurements in a manual way according to their own knowledge and perspectives. A full automatic segmentation method is therefore important for the standardization of heart measurements and to assist in the detection of congenital defects and malformations in clinical practices, as well as for the *3D* (*4D*) heart reconstruction. The created method serves as an excellent framework to assist cardiologist in the echocardiographic examination.

7.1 Future Work

To finalize the algorithm evaluations, it would be important to analyze in a more detailed way the inter operator variability and make statistical studies to prove that the proposed algorithm produces lower divergences than contours drawn by two experts. Another important pursuit is in the frame sequences that can correct dropouts in one image with the following frame.

The fundamental challenge for the future work is the *3D* heart reconstruction. Various possibilities to achieve this goal have been studied based on the available resources. The logical follow up will be the use of a robot arm as a coordinator system: extracting frames and coordinates. The ultrasound probe will be attach on the arm that will transform the data to Cartesian coordinates, placing each pixel in the acquired *2D* images in the correct location in the *3D* volume, supported by interpolation. With an accurate segmentation of an echocardiographic video, it is possible to reconstruct partial structures of the heart using the robot arm from which the extrinsic calibration information (relative pose) can be extracted.

Bibliography

[1] (2010, June 10) Human Heart. [Online]. Available: *http://www.wiziq.com/tutorial/30791-Human-Heart*.

[2] Marieb EN, Hoehn K. *Human Anatomy & Physiology*. Benjamin Cummings, 7 edition, 2008.

[3] (2010, June 8) Disease: Anatomy & Physiology. [Online]. Available: *http://www.micardia.com/CHF-Congestive-Heart-Failure/Structural-heart-disease-and-mitral-prolapses.php*.

[4] Bernier PL, Ota N, Tchervenkov CI, *et al. An invitation to the medical students of the world to join the global coalition to improve care for children and adults with congenital heart disease across the world*. McGill Journal of Medicine, 2008. 11(2):185-190.

[5] Springhouse. *Handbook of Diseases*. Lippincott Williams & Wilkins, 2003.

[6] (2010, June 8) Late Cardiovascular Development. [Online]. Available: *http://php.med.unsw.edu.au/embryology/index.php?title=2009_Lecture_21*.

[7] (2010, June 10) Cardio Ultrasound. [Online]. Available: *http://www.buckeyemedical.com/GE-Vivid-S7-Cardio-Ultrasound*.

[8] Webb AG. *Introduction to Biomedical Imaging*. IEEE Press Series on Biomedical Engineering, 2003.

[9] (2010, June 10) Atlas of Echocardiography. [Online]. Available: *http://www.yale.edu/imaging/echo_atlas/views/index.html*.

[10] Suri JS, Setarehdan SK, Singh S. *Advanced algorithmic approaches to medical image segmentation: state-of-the-art application in cardiology, neurology, mammography and pathology*. Springer-Verlag New York, 2002.

[11] Noble JA. *Ultrasound image segmentation and tissue characterization.* Proceedings of the Institution of Mechanical Engineers: Journal of Engineering in Medicine, 2009. pp. 307-16.

[12] Nillesen MM, Lopata RGP, Gerrits IH, Kapusta L, Huisman HJ, Thijssen JM, Korte CLd. *Segmentation of the Heart Muscle in 3D Pediatric Echocardiographic Images.* Ultrasound in Medicine & Biology. 2007. 33:1453-1462.

[13] Nascimento J, Sanches J. *Ultrasound imaging LV tracking with adaptive window size and automatic hyper-parameter estimation.* 15th IEEE International Conference on Image Processing, 2008. pp. 553-556.

[14] Sudha S, Suresh G, Sukanesh R. *Speckle Noise Reduction in Ultrasound Images Using Context-based Adaptive Wavelet Thresholding.* IETE Journal of Research, 2009. 55:135-143.

[15] Nadernejad E, Karami MR, Sharifzadeh S, Heidari M. *Despeckle Filtering in Medical Ultrasound Imaging.* Contemporary Engineering Sciences, 2009. 2:17-36

[16] Rajpoot K, Noble JA, Grau V, Rajpoot N. *Feature Detection from Echocardiography Images Using Local Phase Information.* Proceedings of 12th Medical Image Understanding and Analysis, 2008. pp. 1-5.

[17] Jarur MC, Mora M. *Heart cavity detection in ultrasound images with SOM.* 5th Mexican international conference on artificial intelligence, 2006. pp. 1211-19.

[18] Suphalakshmi A, Narendran S, Anandhakumar P. *Transtexture based segmentation of echocardiographic images.* International Conference on Computing, Communication and Networking. St. Thomas, 2008. pp. 1-7.

[19] Bansod P, Desai UB, Burkule N. *Multi Frame Guided Local Search for Semiautomatic Endocardial Contour Estimation in Echocardiography Sequences.* 6th International Conference on Information, Communications & Signal Processing. Singapore 2007. pp. 1-5.

[20] Stoitsis J, Golemati S, Kendros S, Nikita KS. *Automated detection of the carotid artery wall in B-mode ultrasound images using active contours initialized by the Hough transform.* 30th Annual International Conference of the IEEE Engineering in Medicine and Biology Society. Vancouver. 2008. pp. 3146-49.

[21] Valdes-Cristerna R, Jimenez JR, Yanez-Suarez O, Lerallut JF, Medina V. *Texture-based echocardiographic segmentation using a non-parametric estimator and an active contour model*. 26th Annual International Conference of the IEEE Engineering in Medicine and Biology Society. San Francisco. 2004. pp. 1806-09.

[22] Cheng J, Foo SW. *Boundary Detection in Echocardiographic Images Using Markovian Level Set Method*. Transactions on Information and Systems. 2007. 8:1292-1300.

[23] Kass M, Witkin A, Terzopoulos D. *Snakes: Active contour models*. International Journal of Computer Vision. 1988. 1:321-31.

[24] Caselles V, Kimmel R, Sapiro G. *Geodesic Active Contours*. International Journal of Computer Vision. 1997. 22:61-79.

[25] Osher S, Sethian JA. *Fronts Propagating with Curvature Dependent Speed: Algorithms Based on Hamilton-Jacobi Formulations*. J. Comput. Phys. 1988. 79:12-49.

[26] Mora M, Tauber C, Batatia H. *Robust Level Set for heart cavities detection in ultrasound images*. Computers in Cardiology 2005. pp.235-38.

[27] Fang W, Chan KL, Fu S, Krishnan SM. *Incorporating temporal information into active contour method for detecting heart wall boundary from echocardiographic image sequence*. Computerized medical imaging and graphics 2008. 32:590-600.

[28] Mumford D, Shah J. *Optimal Approximations by Piecewise Smooth Functions and Associated Variational Problems*. Communications on Pure and Applied Mathematics 1989. 42:577-685.

[29] Chan TF, Vese LA. *Active Contours Without Edges*. IEEE Transactions on Image Processing 2001;10:266-77.

[30] Li C, Kao C-Y, Gore JC, Ding Z. *Minimization of Region-Scalable Fitting Energy for Image Segmentation*. IEEE Transactions on Image Processing 2008. 17:1940-1949.

[31] Paragios N, Deriche R. *Geodesic active regions: A new framework to deal with frame partition problems in computer vision*. Journal of Visual Communication and Image Representation 2002. pp.249-68.

[32] Paragios N. *Variational Methods and Partial Differential Equations in Cardiac Image Analysis*. Proceedings of the 2004 IEEE International Symposium on Biomedical Imaging: From Nano to Macro. Arlington, USA 2004. pp. 17-20.

[33] Zhang Y, Matuszewski BJ, Shark L-K, Moore CJ. *Medical Image Segmentation Using New Hybrid Level-Set Method*. Fifth International Conference BioMedical Visualization: Information Visualization in Medical and Biomedical Informatics: IEEE Computer Society, 2008. pp. 71-76.

[34] Bernard O, Touil B, Gelas A, Prost R, Friboulet D. *A RBF-based multiphase level set method for segmentation in echocardiography using the statistics of the radiofrequency signal*. IEEE International Conference on Image Processing. 2007. 3:157-60.

[35] Oktay AB, Akgul YS. *Echocardiographic contour extraction with local and global priors through boosting and level sets*. IEEE Computer Society Conference on Computer Vision and Pattern Recognition Workshops, CVPR Workshops. Miami 2009. pp. 46-51.

[36] Cheng J, Foo SW, Krishnan SM. *Watershed-presegmented snake for boundary detection and tracking of left ventricle in echocardiographic images*. IEEE Transactions on Information Technology in Biomedicine 2006. 10:414 - 16.

[37] Deka B, Ghosh D. *Watershed Segmentation for Medical Ultrasound Images*. IEEE International Conference on Systems, Man and Cybernetics, SMC. Taipei, 2006. pp. 3186-91.

[38] Lacerda SG, da Rocha AF, Vasconcelos DF, de Carvalho JLA, Sene IG, Camapum JF. *Left Ventricle Segmentation in Echocardiography Using a Radial-Search-Based Image Processing Algorithm*. 30th Annual International Conference of the IEEE Engineering in Medicine and Biology Society, EMBS. Vancouver, 2008. pp. 222-25.

[39] Li L, Fu Y, Bai P, Mao W. *Medical Ultrasound Image Segmentation Based on Improved Watershed Scheme*. 3rd International Conference on Bioinformatics and Biomedical Engineering, 2009. pp. 1-4.

[40] Kovesi P. *Symmetry and Asymmetry from Local Phase*. Tenth Australian Joint Converence on Artificial Intelligence. Perth, 1997. pp. 185-90.

[41] Morrone MC, Owens RA. *Feature detection from local energy*. Pattern Recogn. Lett. 1987. 6:303-13.

[42] Boukerroui D, Noble JA, and Brady M. *On the choice of band-pass quadrature filters*. J. Math. Imaging Vis. 2004. 21:1:53Ű80.

[43] Silva JS, Santos BS, Silva A, Madeira J. *A Level-Set Based Volumetric CT Segmentation Technique: A Case Study with Pulmonary Air Bubbles*. International Conference on Image Analysis and Recognition: Springer-Verlag Berlin, 2004. pp. 68-75.

[44] Santos BS, Ferreira C, Silva JS, Silva A, Teixeira L. *Quantitative Evaluation of a Pulmonary Contour Segmentation Algorithm in X-ray Computed Tomography Images*. Academic Radiology 2004. 11:868-78.

[45] Abdou IE, Pratt WK. *Quantitative Design and Evaluation of Enhancement / Thresholding Edge Detectors*. Proceedings of the IEEE, 1979. 67:5: 753-763.

[46] Silva A, Silva JS, Santos BS, Ferreira C. *Fast pulmonary contour extraction in x-ray CT images: a methodology and quality assessment* Physiology and Function from Multidimensional Images, 2001. 4321:216Ű224.